Inorganic Chemistry

Article

pubs.acs.org/IC

Heteroleptic Chini-Type Platinum Clusters: Synthesis and Characterization of Bis-Phospine Derivatives of $[Pt_{3n}(CO)_{6n}]^{2-}$ (n = 2−4)

Cristiana Cesari, Iacopo Ciabatti, Cristina Femoni, Maria Carmela Iapalucci, Federica Mancini, and Stefano Zacchini*

Dipartimento di Chimica Industriale "Toso Montanari", Università di Bologna, Viale Risorgimento 4, 40136 Bologna, Italy

Supporting Information

ABSTRACT: The reactions of $[Pt_{3n}(CO)_{6n}]^{2-}$ (n = 2−4) homoleptic Chini-type clusters with stoichiometric amounts of $Ph_2PCH_2CH_2PPh_2$ (dppe) result in the heteroleptic Chini-type clusters $[Pt_6(CO)_{10}(dppe)]^{2-}$, $[Pt_9(CO)_{16}(dppe)]^{2-}$, and $[Pt_{12}(CO)_{20}(dppe)_2]^{2-}$. Their formation is accompanied by slight amounts of neutral species such as $Pt_4(CO)_4(dppe)_2$, $Pt_6(CO)_6(dppe)_3$, and $Pt(dppe)_2$. A similar behavior was observed with the chiral ligand R-$Ph_2PCH(Me)CH_2PPh_2$ (R-dppp), and two isomers of $[Pt_9(CO)_{16}(R\text{-dppp})]^{2-}$ were identified. All the new species were spectroscopically characterized by means of IR and ^{31}P NMR, and their structures were determined by single-crystal X-ray diffraction.

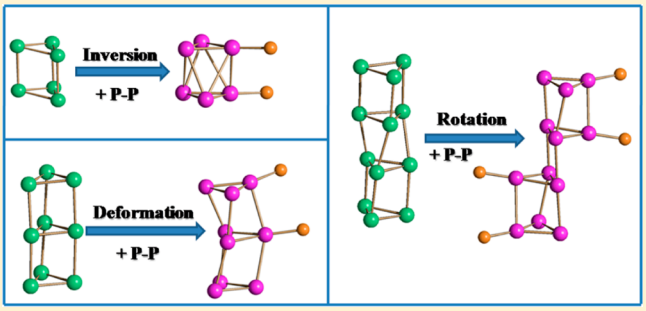

The results obtained are compared to those previously reported for monodentate phosphines, that is, PPh_3, as well as more rigid bidentate ligands, that is, $CH_2{=}C(PPh_2)_2$ (P^P), $CH_2(PPh_2)_2$ (dppm), and o-$C_6H_4(PPh_2)_2$ (dppb). From a structural point of view, functionalization of anionic platinum Chini clusters preserves their triangular Pt_3 units, whereas the overall trigonal prismatic structures present in the homoleptic clusters are readily deformed and transformed upon functionalization. Such transformations may be just local deformations, as found in $[Pt_9(CO)_{16}(dppe)]^{2-}$, $[Pt_9(CO)_{16}(R\text{-dppp})]^{2-}$, $[Pt_{12}(CO)_{22}(PPh_3)_2]^{2-}$, and $[Pt_9(CO)_{16}(PPh_3)_2]^{2-}$; an inversion of the cage from trigonal prismatic to octahedral, as observed in $[Pt_6(CO)_{10}(dppe)]^{2-}$ and $[Pt_6(CO)_{10}(PPh_3)_2]^{2-}$; the reciprocal rotation of two trigonal prismatic units with the loss of a Pt−Pt contact as found in $[Pt_{12}(CO)_{20}(dppe)_2]^{2-}$.

1. INTRODUCTION

After the seminal work of Chini and Longoni,[1,2] $[Pt_{3n}(CO)_{6n}]^{2-}$ (n = 1−8) clusters have represented a milestone in the chemistry of molecular clusters and metal carbonyls. These Chini clusters are composed of a stack of triangular Pt_3 units and can interconvert by simple redox reactions.[3−5] The higher nuclearity clusters (n = 5−8) display the tendency to self-assemble into continuous chains, whose solid-state structures are dependent upon the nature of the charge-balancing cations as well as the sizes of the cluster anions.[6−8] Many of the higher ordered structures display remarkable electric conductive properties, leading to interest in their use as conductive materials.[9−11] Moreover, they can be used as catalysts, as well as precursors of heterogeneous catalysts, metal nanoparticles, and nanowires.[12−16] The thermal decomposition of Chini clusters under milder conditions affords globular platinum nanoclusters and Pt browns,[17−21] whereas their redox condensation with metal carbonyls and salts can lead to bimetallic clusters.[22−24] Conversely, functionalization of Chini clusters via CO substitution has been investigated to a less extent, in view of their tendency to undergo fragmentation, rearrangement, and/or redox reactions upon addition of ligands and nucleophiles.

These are general problems while studying the reactions of metal carbonyl clusters with soft nucleophiles (e.g., CO, PR_3, RCCR, R_2CCR_2, pyridine, NO_2^-, halides), as they may result either in the formation of addition or substitution products, or in cluster breakdown. The nature of the species formed depends on the nucleophile (which may or may not undergo transformation on the cluster surface), the type of metal cluster, and the conditions employed in the reaction.[25−29] It must be remarked that CO substitution with stronger σ-donors such as phosphines becomes less favored when passing from cationic to neutral and, eventually, anionic metal carbonyls. Indeed, most of the examples reported in the literature of CO substitution with PR_3 in anionic carbonyl clusters involve low nuclearity species possessing a robust metal cage, due to the presence of heavier transition metals and/or interstitial heteroatoms.[30−33] More often, larger (and more charged) anionic carbonyl clusters do not react with phosphines, or the reaction results in

Received: November 17, 2016

DOI: 10.1021/acs.inorgchem.6b02750
Inorg. Chem. XXXX, XXX, XXX−XXX

degradation to lower nuclearity species.[11,25,34] In a very few cases, an opposite process has been observed, that is, cluster condensation to higher nuclearity species upon treatment with PR_3.[35]

Within this framework, we recently reported that CO ligands of $[Pt_{3n}(CO)_{6n}]^{2-}$ (n = 2−4) may be partially replaced by PPh_3 leading to the formation of miscellaneous $[Pt_{3n}(CO)_{6n-m}(PPh_3)_m]^{2-}$ (m = 1−3) heteroleptic Chini-type clusters.[36] Conversely, their reactions with rigid bidentate ligands, such as $CH_2{=}C(PPh_2)_2$ (P^P), $CH_2(PPh_2)_2$ (dppm), and o-$C_6H_4(PPh_2)_2$ (dppb), lead to neutral species, that is, $Pt_4(CO)_4(P^P)_2$, $Pt_6(CO)_6(dppm)_3$, and $Pt(dppb)_2$.[37] Herein, we report a detailed spectroscopic (IR and ^{31}P NMR) and structural study of the reactions of Chini clusters $[Pt_{3n}(CO)_{6n}]^{2-}$ (n = 2−4) with a more flexible diphosphine ligand, that is, $Ph_2PCH_2CH_2PPh_2$ (dppe). By using stoichiometric amounts of dppe, it is possible to observe CO/dppe substitution with formation of dppe-functionalized Chini clusters, among which $[Pt_9(CO)_{16}(dppe)]^{2-}$, $[Pt_6(CO)_{10}(dppe)]^{2-}$, and $[Pt_{12}(CO)_{20}(dppe)_2]^{2-}$ were structurally characterized. In addition, the neutral species $Pt_4(CO)_4(dppe)_2$, $Pt_6(CO)_6(dppe)_3$, and $Pt(dppe)_2$ were identified as side products of these reactions. Finally, a similar trend was observed by employing a chiral analogue of dppe, that is, R-$Ph_2PCH(Me)CH_2PPh_2$ (R-dppp). In particular, two isomers of the chiral Chini cluster $[Pt_9(CO)_{16}(R\text{-dppp})]^{2-}$ were obtained and fully characterized.

2. RESULTS AND DISCUSSION

2.1. Reactions of $[Pt_{3n}(CO)_{6n}]^{2-}$ (n = 2,3,4) with dppe.

The reaction of $[Pt_9(CO)_{18}]^{2-}$ with a slight excess of dppe in acetone results, after workup, in the new dianionic cluster $[Pt_9(CO)_{16}(dppe)]^{2-}$, formally in accord to eq 1. The new species was characterized through IR and ^{31}P NMR spectroscopy, and its molecular structure was crystallographically determined as its $[NEt_4]_2[Pt_9(CO)_{16}(dppe)]\cdot 2CH_3COCH_3$ salt.

$$[Pt_9(CO)_{18}]^{2-} + dppe \leftrightarrow [Pt_9(CO)_{16}(dppe)]^{2-} + 2CO \quad (1)$$

Even if formation of $[Pt_9(CO)_{16}(dppe)]^{2-}$ is formally accounted for by eq 1, IR monitoring of the reaction indicates a more complex evolution. Thus, after the addition of dppe to $[Pt_9(CO)_{18}]^{2-}$ under N_2, the IR spectra indicate the formation of a mixture of $[Pt_9(CO)_{18}]^{2-}$ (ν_{CO} 2030(vs), 1855(sh), 1840(s), 1830(sh), 1810(m) cm^{-1}) and $[Pt_6(CO)_{12}]^{2-}$ (ν_{CO} 1995(vs), 1818(m), 1795(s) cm^{-1}) according to eq 2. The (ν_{CO} 1794(vs) cm^{-1}) band of $Pt_6(CO)_6(dppe)_3$ is hidden by the acetone solvent. Then, $[Pt_9(CO)_{16}(dppe)]^{2-}$ (ν_{CO} 2013(vs), 1831(ms) cm^{-1}) is formed after removal of CO under vacuum, probably through a condensation process (eq 3).

$$[Pt_9(CO)_{18}]^{2-} + 1.5dppe \leftrightarrow [Pt_6(CO)_{12}]^{2-} + 0.5Pt_6(CO)_6(dppe)_3 + 3CO \quad (2)$$

$$[Pt_9(CO)_{18}]^{2-} + 2[Pt_6(CO)_{12}]^{2-} + Pt_6(CO)_6(dppe)_3 \leftrightarrow 3[Pt_9(CO)_{16}(dppe)]^{2-} \quad (3)$$

It is likely that equilibria 1−3 are mainly shifted under reduced pressure toward the formation of $[Pt_9(CO)_{16}(dppe)]^{2-}$, which is actually the main product of the reaction after workup. This is confirmed by the fact that $[Pt_9(CO)_{16}(dppe)]^{2-}$ can be directly obtained from the reaction of $[Pt_9(CO)_{18}]^{2-}$ and dppe in acetone, by periodically removing CO in vacuo. In all cases, trace amounts of the neutral $Pt_6(CO)_6(dppe)_3$ cluster may be extracted in CH_2Cl_2 from the crude reaction mixture, in accord to eq 2. $Pt_6(CO)_6(dppe)_3$ was fully characterized by means of IR and ^{31}P NMR spectroscopy and X-ray crystallography. In addition, traces of the neutral complexes $Pt(dppe)_2$ and $Pt_4(CO)_4(dppe)_2$ were sometimes isolated during the workup of the reaction mixture. In particular, formation of $Pt(dppe)_2$ is favored by employing excess of dppe, and this species was, thus, spectroscopically and structurally characterized. Conversely, only a few crystals of $Pt_4(CO)_4(dppe)_2$ were obtained, hampering any further characterization, apart from X-ray crystallography.

The formation of different neutral zerovalent species, that is, $Pt_6(CO)_6(dppe)_3$, $Pt(dppe)_2$, and $Pt_4(CO)_4(dppe)_2$, may be explained assuming that CO/dppe substitution in $[Pt_9(CO)_{18}]^{2-}$ may be followed by elimination of Pt(0) fragments and formation of the lower nuclearity homoleptic Chini cluster $[Pt_6(CO)_{12}]^{2-}$. Elimination may be favored by employing excess dppe. Then, depending on the experimental conditions, the Pt(0) fragments may rearrange affording different neutral species, as mentioned above. A similar trend was previously observed in the case of the reaction of $[Pt_9(CO)_{18}]^{2-}$ with PPh_3, which, depending on the experimental conditions, afforded the substitution products $[Pt_9(CO)_{18-x}(PPh_3)_x]^{2-}$ (x = 1−3) and/or a mixture of $[Pt_6(CO)_{12}]^{2-}$ and $Pt_3(CO)_3(PPh_3)_3$ via elimination of Pt(0).[36] Conversely, in the case of rigid diphosphines such as dppm, P^P, and dppb, only the elimination products were observed, probably because of the instability of the substitution products.[37]

The IR spectrum of $[Pt_9(CO)_{16}(dppe)]^{2-}$ displays both terminal and bridging ν_{CO} bands (2013(vs), 1831(ms) cm^{-1}) at lower frequencies than $[Pt_9(CO)_{18}]^{2-}$ in view of the greater basicity of dppe compared to CO, very close to those previously reported for $[Pt_9(CO)_{16}(PPh_3)_2]^{2-}$ (ν_{CO} 2016(s), 1824(m) cm^{-1}). The $^{31}P\{^1H\}$ NMR spectrum recorded in CD_3CN at 298 K displays two complex resonances centered at δ_P 48.1 and 41.6 ppm (Figure 1; see Scheme 1 for an

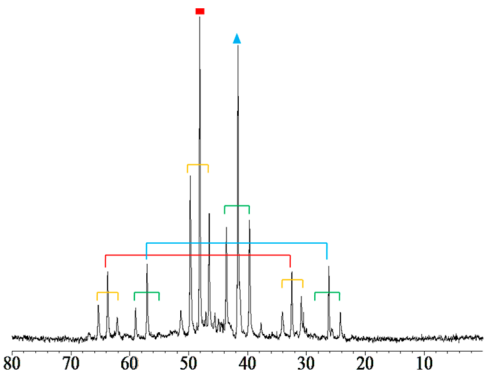

Figure 1. $^{31}P\{^1H\}$ NMR spectrum of $[Pt_9(CO)_{16}(dppe)]^{2-}$ in CD_3CN at 298 K. The main peak of the resonances of the two inequivalent P atoms is indicated with ■, P(1), and ▲, P(2). Arrows are used for the coupling constants: $^1J_{PtP(1)}$, red; $^2J_{PtP(1)}$, yellow; $^1J_{PtP(2)}$, blue; $^2J_{PtP(2)}$, green. The intensities of some Pt satellites are lower than expected because of second-order effects.

DOI: 10.1021/acs.inorgchem.6b02750
Inorg. Chem. XXXX, XXX, XXX−XXX

Scheme 1. Coupling Pattern[a] of the Two P Atoms of $[Pt_9(CO)_{16}(dppe)]^{2-}$

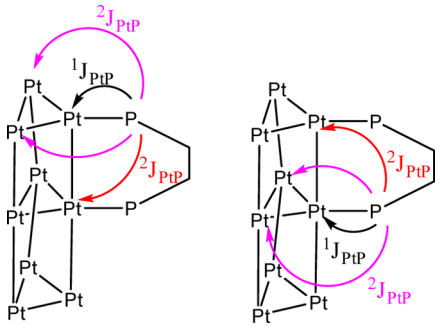

[a] $^3J_{PP}$ is not displayed.

explanation of the observed coupling pattern). Both resonances show a large $^1J_{PtP}$ coupling to one Pt atom (5060 and 4995 Hz for the two resonances, respectively) as well as a very small $^3J_{PP}$ (8 Hz).[38−41] In addition, two very different $^2J_{PtP}$ coupling constants are observed; the larger one (521 and 632 Hz, respectively) corresponds to two equivalent Pt atoms, and the smaller one (17 and 9 Hz, respectively) corresponds to a single Pt atom. On the basis of the crystal structure, the larger $^2J_{PtP}$ values correspond to coupling to the two Pt atoms of the triangle to which the P atom is directly bonded, whereas the smaller $^2J_{PtP}$ values correspond to inter-triangle coupling to the Pt atom bonded to the other P of the same dppe ligand. It is noteworthy that inter-triangle coupling to any nucleus (^{13}C, ^{195}Pt, ^{31}P) is not usually observed in related clusters containing only monodenate ligands, that is, $[Pt_9(CO)_{18}]^{2-}$, $[Pt_9(CO)_{17}(PPh_3)]^{2-}$, and $[Pt_9(CO)_{16}(PPh_3)_2]^{2-}$.[5] Thus, it is likely that the small inter-triangle $^2J_{PtP}$ coupling observed in $[Pt_9(CO)_{16}(dppe)]^{2-}$ is due to the bidentate nature of dppe. The assignment of the $^{31}P\{^1H\}$ NMR spectrum is fully corroborated by simulation with gNMR 5.0.6.0 (Figures S.1 and S.2 in Supporting Information).[42]

The neutral $Pt_6(CO)_6(dppe)_3$ cluster is closely related to the previously reported $Pt_6(CO)_6(dppm)_3$ and $Pt_3(CO)_3(PPh_3)_3$ species.[43,44] It displays a ν_{CO} band at 1797 cm^{-1} corresponding to the six μ-CO ligands. The $^{31}P\{^1H\}$ NMR spectrum recorded in CD_2Cl_2 at 298 K (Figure 2) shows a complex resonance at δ_P 52.1 ppm ($^1J_{PtP}$ = 4825 Hz (1Pt), $^2J_{PtP}$ = 527 Hz (2Pt), $^3J_{PP}$ = 62 Hz (2P)) corresponding to a second-order AA′A″A‴A⁗A⁗″XX′X″X‴X⁗X⁗″ system only partially resolved (see Figure S.3 for the simulated spectrum). Conversely, the mononuclear complex $Pt(dppe)_2$ shows a first-order AX spectrum as indicated by a pseudotriplet centered at δ_P 29.8 ppm ($^1J_{Pt-P}$ = 3734 Hz) in the $^{31}P\{^1H\}$ NMR spectrum (Figure S.4).

In a similar manner, the reaction of $[Pt_{12}(CO)_{24}]^{2-}$ with 1 equiv of dppe results immediately in a mixture of $[Pt_{12}(CO)_{24}]^{2-}$ and $[Pt_9(CO)_{18}]^{2-}$, as evidenced by IR spectroscopy. Nonetheless, as above, after workup (see Experimental) a new species displaying ν_{CO} bands at 2036(vs) and 1839(s) cm^{-1} is formed. Analogously to the above-described reaction involving $[Pt_9(CO)_{18}]^{2-}$ and dppe, and based on the similarity of the IR spectrum of the new species with that reported for $[Pt_{12}(CO)_{22}(PPh_3)_2]^{2-}$, the new species may be formulated as $[Pt_{12}(CO)_{22}(dppe)]^{2-}$. Unfortunately, all attempts to crystallize it failed. The ^{31}P NMR spectra of the purported $[Pt_{12}(CO)_{22}(dppe)]^{2-}$ dianion recorded in the temperature range of 213−298 K display always a broad resonance centered at 43 ppm (line width ca. 150 Hz) with $^1J_{Pt-P}$ = 5020 Hz and $^2J_{Pt-P}$ = 545 Hz. This indicates a fluxional behavior at all the temperatures considered. Formation of $[Pt_{12}(CO)_{22}(dppe)]^{2-}$ is accompanied by neutral side-products, such as $Pt_6(CO)_6(dppe)_3$ and $Pt(dppe)_2$.

Conversely, the reaction of $[Pt_{12}(CO)_{24}]^{2-}$ with 2 equiv of dppe affords in a few minutes a dark red solution containing $[Pt_9(CO)_{18}]^{2-}$ as the major species together with traces of unreacted $[Pt_{12}(CO)_{24}]^{2-}$ (by IR). In this case, after removal of the solvent in vacuo and dissolution of the solid in CH_3CN, a green solution of the new cluster $[Pt_{12}(CO)_{20}(dppe)_2]^{2-}$ was obtained. Its formation is accompanied by neutral species as above, which may be separated based on their different solubilities in organic solvents. The structure of this new heteroleptic anionic cluster was fully determined by X-ray crystallography as its $[NMe_3(CH_2Ph)]_2[Pt_{12}(CO)_{20}(dppe)_2]\cdot CH_3CN$ and $[NMe_4]_2[Pt_{12}(CO)_{20}(dppe)_2]\cdot 2CH_3CN$ salts. These crystals display ν_{CO} bands at 2008(vs), 1974(m), 1854(w), and 1810(s) cm^{-1} in nujol mull and at 2015(vs), 1854(w), 1828(s), and 1807(m) in CH_3CN solution. A downshift of 25−30 cm^{-1} compared to the starting $[Pt_{12}(CO)_{24}]^{2-}$ is observed for both terminal and edge-bridging ν_{CO} bands, in agreement with substitution of four CO ligands with two bidendate dppe. The ^{31}P NMR spectrum of $[Pt_{12}(CO)_{20}(dppe)_2]^{2-}$ (Figure 3) is fully consistent with its solid-state structure (see Section 2.3), which contains two equivalent dppe ligands, whereas the two P atoms within each dppe are not equivalent. As a result, the pattern of the ^{31}P NMR spectrum of $[Pt_{12}(CO)_{20}(dppe)_2]^{2-}$ is similar to that of $[Pt_9(CO)_{16}(dppe)]^{2-}$. Thus, it displays two resonances at δ_P

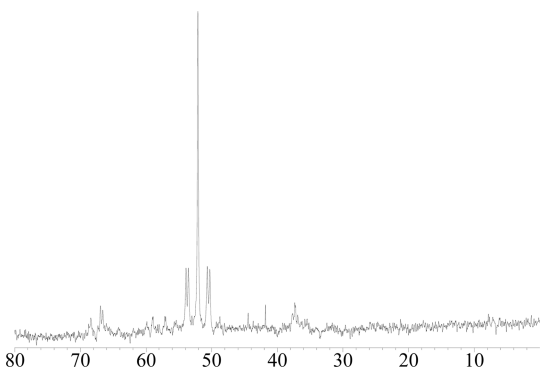

Figure 2. $^{31}P\{^1H\}$ NMR spectrum of $Pt_6(CO)_6(dppe)_3$ in CD_2Cl_2 at 298 K.

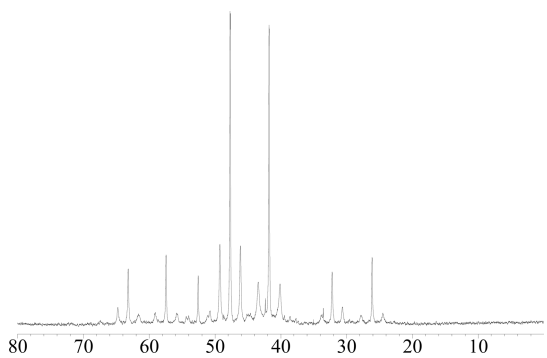

Figure 3. $^{31}P\{^1H\}$ NMR spectrum of $[Pt_{12}(CO)_{20}(dppe)_2]^{2-}$ in CD_3CN at 298 K.

DOI: 10.1021/acs.inorgchem.6b02750
Inorg. Chem. XXXX, XXX, XXX−XXX

47.7 and 41.7 (see Figures S.5 and S.6 for the simulated spectra). Both resonances show $^1J_{PtP}$ coupling to one Pt atom (5024 and 5076 Hz, respectively), a larger $^2J_{PtP}$ coupling constant to two Pt atoms (513 and 528 Hz, respectively), a smaller $^2J_{PtP}$ coupling constant to one Pt atom (19 and 17 Hz, respectively), and a very small $^3J_{PP}$ (8 Hz).

$[Pt_6(CO)_{12}]^{2-}$ apparently does not react with a slight excess (1−4 equiv) of dppe under N_2, whereas $[Pt_6(CO)_{10}(dppe)]^{2-}$ is formed in good yields under vacuum. It is likely that equilibrium 4 is shifted toward the formation of $[Pt_6(CO)_{10}(dppe)]^{2-}$ only after removing the CO; otherwise, $[Pt_6(CO)_{12}]^{2-}$ is the main species present in solution. The substitution reaction is always accompanied by formation of neutral compounds such as $Pt_6(CO)_6(dppe)_3$ and $Pt(dppe)_2$, which were identified on the basis of IR, ^{31}P NMR spectroscopy, and X-ray crystallography (see above).

$$[Pt_6(CO)_{12}]^{2-} + dppe \leftrightarrow [Pt_6(CO)_{10}(dppe)]^{2-} + 2CO \quad (4)$$

The crystal structure of the new cluster $[Pt_6(CO)_{10}(dppe)]^{2-}$ was determined as its $[NMe_4]_2[Pt_6(CO)_{10}(dppe)]$ and $[NEt_4]_2[Pt_6(CO)_{10}(dppe)]$ salts. These crystals show ν_{CO} bands at 1975(s), 1955(vs), 1756(s), and 1732(ms) cm^{-1} in nujol mull and at 1976(vs), 1784(s), and 1765(s) in CH_3CN solution. In keeping with the solid-state structure, the ^{31}P NMR spectrum of $[Pt_6(CO)_{10}(dppe)]^{2-}$ displays a single resonance at δ_P 51.2 ppm, in view of the equivalence of the two P atoms of the unique dppe ligand (Figure 4). The following coupling constants are observed: $^1J_{PtP}$ = 5086 Hz to one Pt atom; $^2J_{PtP}$ = 550 Hz to two Pt atoms; $^2J_{PtP}$ = 21 Hz to one Pt atom (see Figures S.7 and S.8 for the simulated spectra).

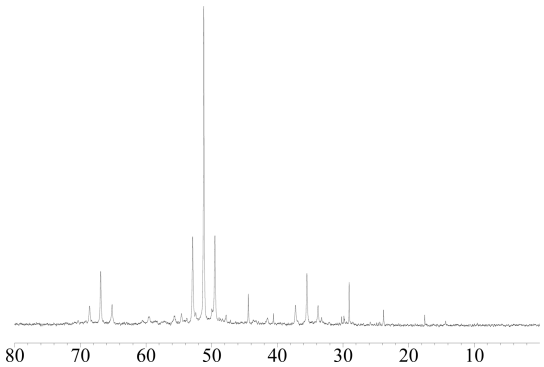

Figure 4. $^{31}P\{^1H\}$ NMR spectrum of $[Pt_6(CO)_{10}(dppe)]^{2-}$ in DMF/CD_3CN at 298 K.

It is noteworthy that the oxidation of $[Pt_6(CO)_{10}(dppe)]^{2-}$ with stoichiometric amounts of $HBF_4{\cdot}Et_2O$ results in the formation of $[Pt_{12}(CO)_{20}(dppe)_2]^{2-}$ as indicated by IR spectroscopy. Conversely, the oxidation of the homoleptic analogue $[Pt_6(CO)_{12}]^{2-}$ affords $[Pt_9(CO)_{18}]^{2-}$ via the formal addition of a single triangular unit. Indeed, this is the general behavior observed for the oxidation of homoleptic Chini clusters $[Pt_{3n}(CO)_{6n}]^{2-}$ resulting in $[Pt_{3(n+1)}(CO)_{6(n+1)}]^{2-}$ species.[1−4,7,8] The same behavior was observed for all the PPh_3 derivatives previously reported, as well as the other species herein described that contain a single dppe ligand. It is noteworthy that a mono-anionic $[Pt_3(\mu\text{-}CO)_3(CNR)_3]^-$ (R = 2,6-(2,6-(*i*-Pr)$_2C_6H_3)_2C_6H_3$) cluster with terminal isocyanide ligands was recently reported, supporting the idea that oxidation of Chini clusters proceeds via transient monoradical intermediates and exchange on triangular units.[6] It is likely that the unique behavior observed for the oxidation of $[Pt_6(CO)_{10}(dppe)]^{2-}$ is due to the fact that both its triangular units are held together by the bridging dppe and it does not contain any unsubstituted $Pt_3(CO)_6$ unit as, conversely, for all the other species reported. Thus, its oxidation cannot proceed via removal of one electron and formal addition of one $Pt_3(CO)_6$ unit, but the monoelectronic oxidation is followed by dimerization resulting in $[Pt_{12}(CO)_{20}(dppe)_2]^{2-}$ (Scheme 2). Finally, it must be remarked that the addition of excess $HBF_4{\cdot}Et_2O$ to $[Pt_6(CO)_{10}(dppe)]^{2-}$ results in the formation of a complex mixture of degradation products, among which $[Pt(dppe)_2][Pt_{12}(CO)_{24}]{\cdot}2DMF$ (DMF = dimethylformamide) was crystallographically identified (Figure S.9).

2.2. Reactions of $[Pt_{3n}(CO)_{6n}]^{2-}$ (n = 2,3,4) with R-dppp. The reactions of $[Pt_{3n}(CO)_{6n}]^{2-}$ (n = 2,3,4) with R-dppp are very similar to those described in the previous section involving dppe. A complication arises from the fact that the two P atoms of R-dppp are not equivalent, and thus, different isomers may be formed upon coordination to the clusters. This point is well-exemplified by the reaction of $[Pt_9(CO)_{18}]^{2-}$ with 1 equiv of R-dppp which, after workup, results in the $[Pt_9(CO)_{16}(R\text{-}dppp)]^{2-}$ cluster. This compound displays an IR spectrum very similar to $[Pt_9(CO)_{16}(dppe)]^{2-}$. Its molecular structure was determined as $[NEt_4]_2[Pt_9(CO)_{16}(R\text{-}dppp)]{\cdot}2CH_3COCH_3$, which actually contains a 1:1 mixture of two isomers, differing in the orientation of the R-dppp ligand with respect to the cluster (Scheme 3). Both isomers contain two inequivalent P atoms, resulting in a very complex ^{31}P NMR spectrum (Figure 5) that displays four main resonances with coupling patterns similar to $[Pt_9(CO)_{16}(dppe)]^{2-}$. The assignment of the $^{31}P\{^1H\}$ NMR spectrum is fully corroborated by simulation with gNMR 5.0.6.0 (Figure S.10).[42] Thus, isomer I

Scheme 2. Proposed Mechanism for the Oxidation of $[Pt_6(CO)_{10}(dppe)]^{2-}$ to $[Pt_{12}(CO)_{20}(dppe)_2]^{2-}$

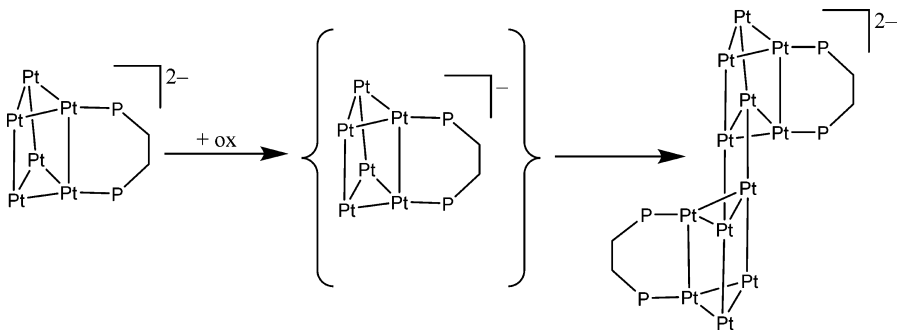

DOI: 10.1021/acs.inorgchem.6b02750
Inorg. Chem. XXXX, XXX, XXX−XXX

Scheme 3. Two Isomers of $[Pt_9(CO)_{16}(R\text{-dppp})]^{2-}$

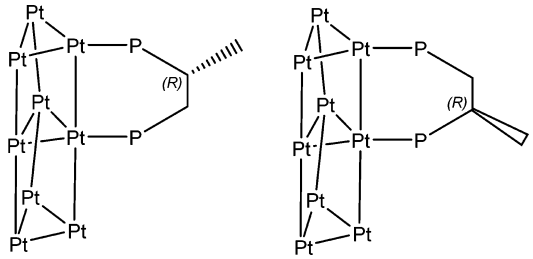

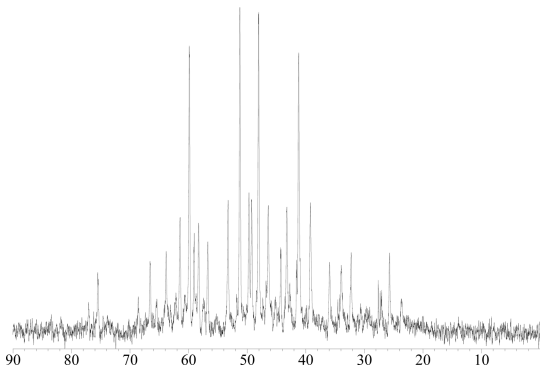

Figure 5. $^{31}P\{^1H\}$ NMR spectrum of $[Pt_9(CO)_{16}(R\text{-dppp})]^{2-}$ in CD_3COCD_3 at 298 K.

displays two resonances at δ_P (ppm) 59.8 ($^1J_{PtP}$ = 5037 Hz (1Pt), $^2J_{PtP}$ = 517 Hz (2Pt), $^3J_{PP}$ = 11 Hz) and 48.0 ($^1J_{PtP}$ = 4436 Hz (1Pt), $^2J_{PtP}$ = 529 Hz (2Pt), $^3J_{PP}$ = 11 Hz). Conversely, Isomer II shows two resonances at 51.2 ($^1J_{PtP}$ = 4944 Hz (1Pt), $^2J_{PtP}$ = 649 Hz (2Pt), $^3J_{PP}$ = 10 Hz), 41.2 ($^1J_{PtP}$ = 5033 Hz (1Pt), $^2J_{PtP}$ = 648 Hz (2Pt), $^3J_{PP}$ = 10 Hz). By comparison, the free R-dppp ligand displays two resonances at δ (ppm) 0.5 and −21.5 with $^3J_{PP}$ = 20 Hz.

The reaction of $[Pt_6(CO)_{12}]^{2-}$ with R-dppp, under conditions similar to those employed in the case of dppe, affords, after workup, $[Pt_6(CO)_{10}(R\text{-dppp})]^{2-}$ as evidenced by IR and ^{31}P NMR spectroscopies (Figure S.11). In this case, a single product is formed in view of the fact that the hexanuclear cluster contains two equivalent triangular units. $[Pt_6(CO)_{10}(R\text{-dppp})]^{2-}$ displays two inequivalent P atoms with δ_P (ppm) 61.4 ($^1J_{PtP}$ = 4937 Hz (1Pt), $^2J_{PtP}$ = 540 Hz (2Pt), $^3J_{PP}$ = 5 Hz) and 49.0 ($^1J_{PtP}$ = 5032 Hz (1Pt), $^2J_{PtP}$ = 564 Hz (2Pt), $^3J_{PP}$ = 5 Hz).

Finally, the reaction of $[Pt_{12}(CO)_{24}]^{2-}$ with R-dppp is rather complicated, and only a few hypotheses may be drawn on the basis of spectroscopic data. As in the case of the analogous reactions with dppe, it seems that both $[Pt_{12}(CO)_{22}(R\text{-dppp})]^{2-}$ and $[Pt_{12}(CO)_{20}(R\text{-dppp})_2]^{2-}$ may be formed, depending on the stoichiometry of the reaction. Unfortunately, it has not been possible to obtain the crystal structures of these clusters. In the case of $[Pt_{12}(CO)_{22}(R\text{-dppp})]^{2-}$, its ^{31}P NMR spectrum shows two very broad resonances at 50 and 35 ppm, indicative of a fluxional behavior, as previously described for $[Pt_{12}(CO)_{22}(dppe)]^{2-}$. Conversely, the purported $[Pt_{12}(CO)_{20}(R\text{-dppp})_2]^{2-}$ displays a rather complex and ill-defined ^{31}P NMR spectrum. This may be due to the presence of side products as well as the fact that three different isomers of $[Pt_{12}(CO)_{20}(R\text{-dppp})_2]^{2-}$ should be formed in a statistical 2:1:1 ratio, based on the orientation of the Me groups of the two R-dppp ligands compared to the four Pt_3 units of the cluster.

2.3. Crystal Structures of the Heteroleptic Chini-Type Clusters. The molecular structures of $[Pt_9(CO)_{16}(dppe)]^{2-}$, $[Pt_9(CO)_{16}(R\text{-dppp})]^{2-}$, $[Pt_6(CO)_{10}(dppe)]^{2-}$, and $[Pt_{12}(CO)_{20}(dppe)_2]^{2-}$, as determined as their $[NEt_4]_2[Pt_9(CO)_{16}(dppe)]\cdot 2CH_3COCH_3$, $[NEt_4]_2[Pt_9(CO)_{16}(R\text{-dppp})]\cdot 2CH_3COCH_3$, $[NMe_4]_2[Pt_6(CO)_{10}(dppe)]$, $[NEt_4]_2[Pt_6(CO)_{10}(dppe)]$, $[NMe_3(CH_2Ph)]_2[Pt_{12}(CO)_{20}(dppe)_2]\cdot CH_3CN$, and $[NMe_4]_2[Pt_{12}(CO)_{20}(dppe)_2]\cdot 2CH_3CN$ salts, are represented in Figures 6−9, whereas their main bonding parameters are

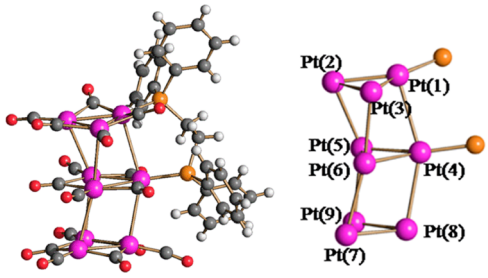

Figure 6. Molecular structure of $[Pt_9(CO)_{16}(dppe)]^{2-}$ (Pt, purple; P, orange; O, red; C, gray; H, white).

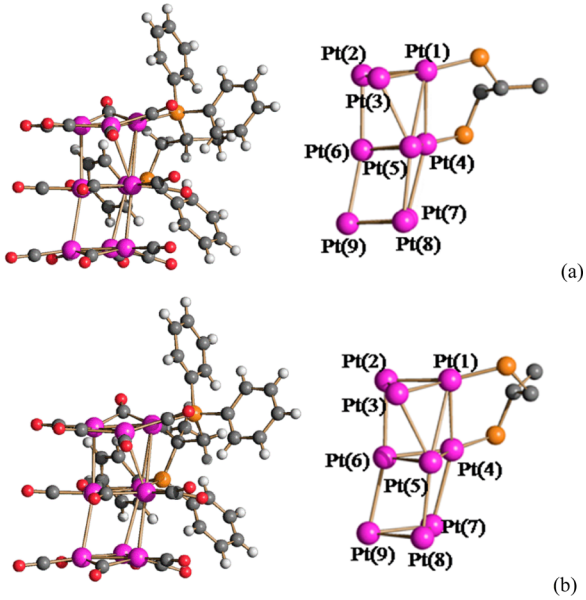

Figure 7. Molecular structure of the two isomers (a, b) of $[Pt_9(CO)_{16}(R\text{-dppp})]^{2-}$ (Pt, purple; P, orange; O, red; C, gray; H, white).

compared in Table 1 to those of the parent $[Pt_{12}(CO)_{24}]^{2-}$, $[Pt_9(CO)_{18}]^{2-}$, and $[Pt_6(CO)_{12}]^{2-}$,[1,2] as well as the related $[Pt_{12}(CO)_{22}(PPh_3)_2]^{2-}$, $[Pt_9(CO)_{16}(PPh_3)_2]^{2-}$, and $[Pt_6(CO)_{10}(PPh_3)_2]^{2-}$.[36] In drawing Figures 6−9 it was arbitrarily decided to represent Pt−Pt bonds up to 3.36 Å, which is slightly below twice the van der Waals radius of Pt and ca. 20% greater than twice its covalent radius (covalent radius 1.36 Å; van der Waals radius 1.72 Å).[45]

The molecular structure of $[Pt_9(CO)_{16}(dppe)]^{2-}$ (Figure 6 and Table 1) can be formally obtained from that of $[Pt_9(CO)_{18}]^{2-}$, after replacing two terminal CO ligands, one in the inner and one in one of the outer Pt_3 triangular units, with dppe. It is noteworthy that in the case of the related $[Pt_9(CO)_{16}(PPh_3)_2]^{2-}$, the two monodentate PPh_3 ligands

DOI: 10.1021/acs.inorgchem.6b02750
Inorg. Chem. XXXX, XXX, XXX−XXX

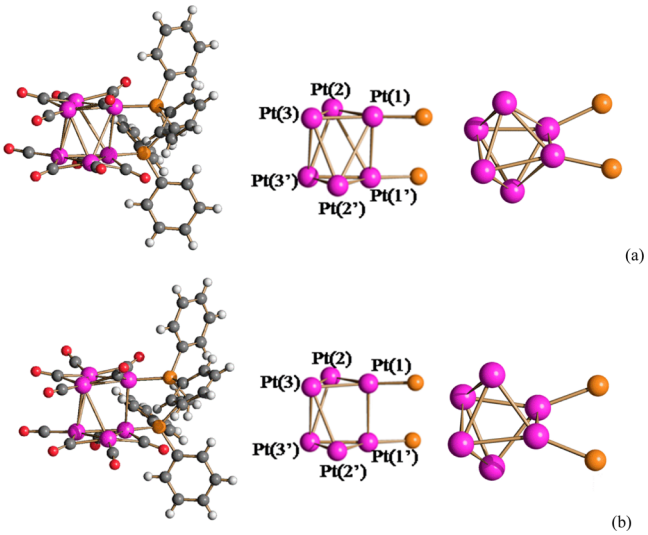

Figure 8. Molecular structure of $[Pt_6(CO)_{10}(dppe)]^{2-}$ as found in (a) $[NEt_4]_2[Pt_6(CO)_{10}(dppe)]$ and (b) $[NMe_4]_2[Pt_6(CO)_{10}(dppe)]$ (Pt, purple; P, orange; O, red; C, gray; H, white).

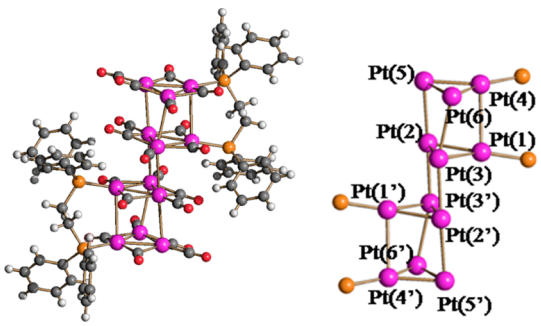

Figure 9. Molecular structure of $[Pt_{12}(CO)_{20}(dppe)_2]^{2-}$ (Pt, purple; P, orange; O, red; C, gray; H, white).

were found bonded to two different external triangles to release steric repulsion. Overall, $[Pt_9(CO)_{16}(dppe)]^{2-}$ retains the trigonal prismatic structure of the parent homoleptic Chini cluster, even if the Pt_6 trigonal prism bonded to dppe is considerably distorted. This causes an elongation of the inter-triangular Pt−Pt contacts of $[Pt_9(CO)_{16}(dppe)]^{2-}$ [2.9968(9)−3.2744(9) Å; average 3.114(2) Å] compared to $[Pt_9(CO)_{18}]^{2-}$ [3.04(2)−3.06(2) Å; average 3.05(4) Å] and $[Pt_9(CO)_{16}(PPh_3)_2]^{2-}$ [3.0015(9)−3.1098(8) Å; average 3.043(2) Å]. The shortest diagonal Pt−Pt contact in the distorted trigonal prismatic dppe-substituted cage is Pt(1)−Pt(5) [3.4360(10) Å], indicating an incipient octahedral structure. Conversely, the intra-triangular contacts [2.6485(10)−2.6841(9) Å; average 2.667(3) Å] are in keeping with other homoleptic and heteroleptic Chini-type clusters. The structural differences observed for the $[Pt_9(CO)_{18}]^{2-}$, $[Pt_9(CO)_{16}(PPh_3)_2]^{2-}$, and $[Pt_9(CO)_{16}(dppe)]^{2-}$ clusters are attributable to both steric and electronic effects. It may be also the case that the phosphine-substituted clusters partially attempt to align the π^* systems of bridging COs, thereby leading to a distortion of stacked rings.

The structure of $[Pt_9(CO)_{16}(R\text{-dppp})]^{2-}$ (Figure 7 and Table 1) is very similar to that of $[Pt_9(CO)_{16}(dppe)]^{2-}$. The main difference is that, in view of the asymmetric nature of R-dppp, two different isomers are present in a 1:1 ratio in the solid-state structure. This is because the P atom close to the Me group in R-dppp may statistically attack the external or internal Pt_3 units, and both orientations are energetically equivalent. It is also noteworthy that the distortion of the trigonal prismatic Pt_6 unit bonded to R-dppp is greater than in the case of dppe, with the shortest diagonal Pt−Pt contact, which is now weakly bonding [Pt(1)−Pt(5) 3.357(2) Å].

$[Pt_6(CO)_{10}(dppe)]^{2-}$ displays a distorted octahedral geometry (Figure 8 and Table 1), in contrast to the parent $[Pt_6(CO)_{12}]^{2-}$, which adopts a trigonal prismatic structure. Moreover, some slight differences in the octahedral core of $[Pt_6(CO)_{10}(dppe)]^{2-}$ were found in the two $[NMe_4]_2[Pt_6(CO)_{10}(dppe)]$ and $[NEt_4]_2[Pt_6(CO)_{10}(dppe)]$ salts. A similar behavior was observed for the related $[Pt_6(CO)_{10}(PPh_3)_2]^{2-}$ cluster.[36] In particular, the Pt_6 cage of $[Pt_6(CO)_{10}(dppe)]^{2-}$ displays six inter-triangular Pt−Pt bonding contacts in $[NEt_4]_2[Pt_6(CO)_{10}(dppe)]$ [3.0437(10)−3.359(2) Å; average 3.202(2) Å] as expected for an octahedron, even if some of them are slightly elongated. Conversely, in the case of $[NMe_4]_2[Pt_6(CO)_{10}(dppe)]$, there are four inter-triangular Pt−Pt contacts [2.9839(4)−3.1797(3) Å; average 3.1285(8) Å] at bonding distance, whereas the remaining two distances are nonbonding [Pt(1)−Pt(2′) and Pt(1′)−Pt(2) 3.526(2) Å]. These differences between the two salts can be ascribed to packing forces due to the presence of different cations. Similarly, analogous differences in the distorted octahedral structures of $[Pt_6(CO)_{10}(PPh_3)_2]^{2-}$ were observed due to different packing effects resulting from inclusion of tetrahydrofuran (THF) in one salt. This points out that the inter-triangular bonds are rather weak and easily deformed by small changes in the van der Waals forces within the crystals.

Finally, the structure of $[Pt_{12}(CO)_{20}(dppe)_2]^{2-}$ was determined as two different salts, that is, $[NMe_3(CH_2Ph)]_2[Pt_{12}(CO)_{20}(dppe)_2]\cdot CH_3CN$ and $[NMe_4]_2[Pt_{12}(CO)_{20}(dppe)_2]\cdot 2CH_3CN$, displaying very similar geometries and bonding parameters (Figure 9 and Table 1). $[Pt_{12}(CO)_{20}(dppe)_2]^{2-}$ adopts an unprecedented structure for a Chini-type cluster. Indeed, it is composed of two trigonal prismatic $[Pt_6(CO)_{10}(dppe)]$ units rotated of 180° and joined by the two symmetry-equivalent Pt(2)−Pt(3′) and Pt(2′)−Pt(3) bonds [2.9765(8) and 2.9728(5) Å, for the two salts, respectively]. As a consequence, there is one μ-CO ligand per $[Pt_6(CO)_{10}(dppe)]$ unit, which sits above one Pt atom of the second $[Pt_6(CO)_{10}(dppe)]$ unit [Pt(1)···C(O) 3.324(14) and 3.286(10) Å, for the two salts, respectively].

2.4. Crystal Structures of the Neutral Side-Products. The molecular structures of the neutral $Pt_4(CO)_4(dppe)_2$, $Pt_6(CO)_6(dppe)_3$, and $Pt(dppe)_2$ species will be briefly discussed, since they closely resemble those of analogous compounds previously reported with other diphosphine ligands.

Thus, the structure of $Pt_4(CO)_4(dppe)_2$ is closely related to $Pt_4(CO)_4(P^\wedge P)_2$[37] and consists of a tetrahedral Pt_4 core elongated along its C_2 axis (Figure 10). The two edges of the elongated tetrahedron perpendicular to the C_2 axis are bridged by two dppe ligands, and the coordination sphere of the cluster is completed by four terminal CO ligands, one per each Pt atom. The six Pt−Pt contacts are divided into three sets consisting of two bonds each. The shortest contacts are those bridged by the dppe ligands [2.5771(3) and 2.5890(3) Å] and perpendicular to the elongation axis. The two bonds almost parallel to the C_2 axis [2.6165(3) and 2.6228(3) Å] have intermediate values. Conversely, the two diagonals of the elongated tetrahedron [2.9995(3) and 3.0164(3) Å] are the

DOI: 10.1021/acs.inorgchem.6b02750
Inorg. Chem. XXXX, XXX, XXX−XXX

Table 1. Main Bond Distances of $[Pt_{12}(CO)_{20}(dppe)_2]^{2-}$, $[Pt_9(CO)_{16}(dppe)]^{2-}$, $[Pt_9(CO)_{16}(R\text{-}dppp)]^{2-}$, and $[Pt_6(CO)_{10}(dppe)]^{2-}$ Compared to the Parent $[Pt_{12}(CO)_{24}]^{2-}$, $[Pt_9(CO)_{18}]^{2-}$, and $[Pt_6(CO)_{12}]^{2-}$, and the PPh_3-Substituted Clusters $[Pt_{12}(CO)_{22}(PPh_3)_2]^{2-}$, $[Pt_9(CO)_{16}(PPh_3)_2]^{2-}$, and $[Pt_6(CO)_{10}(PPh_3)_2]^{2-}$

	Pt−Pt intra-triangular	Pt−Pt inter-triangular[a]	Pt−P
$[Pt_{12}(CO)_{20}(dppe)_2]^{2-}$ [b]	2.6520(8)−2.6795(7)	2.9765(8)−3.1939(8)	2.254(4)−2.272(4)
	average 2.669(2)	average 3.068(2)	average 2.263(6)
$[Pt_{12}(CO)_{20}(dppe)_2]^{2-}$ [c]	2.6513(5)−2.6780(5)	2.9728(5)−3.2075(5)	2.251(2)−2.270(2)
	average 2.6671(12)	average 3.0632(12)	average 2.260(3)
$[Pt_{12}(CO)_{22}(PPh_3)_2]^{2-}$ [d]	2.6539(9)−2.6756(9)	3.0184(9)−3.2067(11)	2.281(4)
	average 2.666(2)	average 3.086(2)	
$[Pt_{12}(CO)_{24}]^{2-}$ [e]	2.6587(5)−2.6707(5)	3.0465(5)−3.0597(5)	
	average 2.6656(12)	average 3.0535(12)	
$[Pt_9(CO)_{16}(dppe)]^{2-}$	2.6485(10)−2.6841(9)	2.9968(9)−3.2744(9)	2.263(4)−2.282(4)
	average 2.667(3)	average 3.114(2)	average 2.272(6)
$[Pt_9(CO)_{16}(R\text{-}dppp)]^{2-}$	2.64913)−2.6843(12)	3.0088(14)−3.357(2)	2.277(6)−2.280(6)
	average 2.667(4)	average 3.127(4)	average 2.278(8)
$[Pt_9(CO)_{16}(PPh_3)_2]^{2-}$ [d]	2.6597(8)−2.6814(9)	3.0015(9)−3.1098(8)	2.265(4)−2.287(4)
	average 2.670(2)	average 3.043(2)	average 2.276(6)
$[Pt_9(CO)_{18}]^{2-}$ [e]	2.65(2)−2.67(8)	3.04(2)−3.06(2)	
	average 2.66(9)	average 3.05(4)	
$[Pt_6(CO)_{10}(dppe)]^{2-}$ [f]	2.6513(3)−2.6839(3)	2.9839(4)−3.1797(3)	2.2456(13)
	average 2.6625(9)	average 3.1285(8)[g]	
$[Pt_6(CO)_{10}(dppe)]^{2-}$ [h]	2.6573(8)−2.6758(8)	3.0437(10)−3.359(2)	2.251(4)
	average 2.6644(14)	average 3.202(2)[i]	
$[Pt_6(CO)_{10}(PPh_3)_2]^{2-}$ [j]	2.6558(6)−2.6743(6)	3.0353(6)[k]	2.240(3)
	average 2.6644(10)		
$[Pt_6(CO)_{10}(PPh_3)_2]^{2-}$ [l]	2.6584(6)−2.6787(6)	3.1380(6)−3.2079(6)	2.247(3)
	average 2.6694(10)	average 3.1729(8)[m]	
$[Pt_6(CO)_{12}]^{2-}$ [e]	2.644(7)−2.659(3)	3.026(16)−3.049(17)	
	average 2.653(10)	average 3.03(3)	

[a]Only Pt−Pt interactions ≤3.36 Å were included (see text). [b]As found in $[NMe_3(CH_2Ph)]_2[Pt_{12}(CO)_{20}(dppe)_2]\cdot CH_3CN$. [c]As found in $[NMe_4]_2[Pt_{12}(CO)_{20}(dppe)_2]\cdot 2CH_3CN$. [d]From ref 36. [e]From ref 12. [f]As found in $[NMe_4]_2[Pt_6(CO)_{10}(dppe)]$. [g]Four inter-triangular Pt−Pt bonding contacts are present. The remaining two Pt−Pt contacts are 3.526(2) Å. [h]As found in $[NEt_4]_2[Pt_6(CO)_{10}(dppe)]$. [i]Six inter-triangular Pt−Pt bonding contacts are present. [j]As found in $[NBu_4]_2[Pt_6(CO)_{10}(PPh_3)_2]$. From ref 36. [k]Three sets of inter-triangular Pt−Pt contacts are present: 3.0353(6), 3.3581(6), 3.5070(6) Å. From ref 36. [l]As found in $[NBu_4]_2[Pt_6(CO)_{10}(PPh_3)_2]\cdot 2THF$. From ref 36. [m]Three sets of inter-triangular Pt−Pt contacts are present: 3.1380(6), 3.2079(6), 3.4310(6) Å. From ref 36.

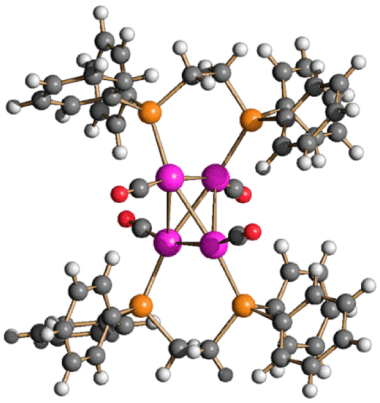

Figure 10. Molecular structure of $Pt_4(CO)_4(dppe)_2$ (Pt, purple; P, orange; O, red; C, gray; H, white).

loosest Pt−Pt contacts. The cluster possesses 56 CVE as predicted for a Pt_4 tetrahedral cluster on the basis of theoretical considerations.[46]

$Pt_6(CO)_6(dppe)_3$ is isostructural with $Pt_6(CO)_6(dppm)_3$,[43] being composed of a Pt_6 trigonal prismatic core possessing D_{3h} symmetry to which are coordinated six μ-CO and three μ-dppe ligands (Figure 11 and Table 2). The structure of the cluster and the bonding parameters closely resemble those of $[Pt_6(CO)_{12}]^{2-}$ and $Pt_6(CO)_6(dppm)_3$.

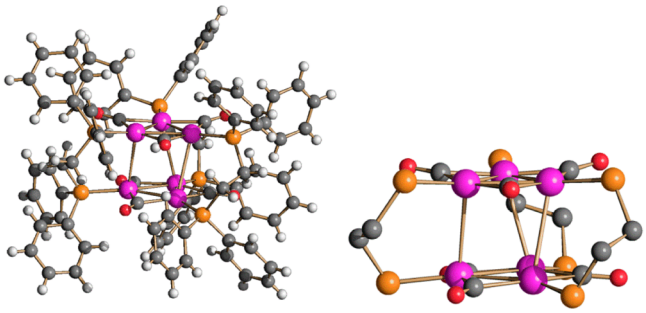

Figure 11. Molecular structure of $Pt_6(CO)_6(dppe)_3$ (Pt, purple; P, orange; C, gray, O, red).

Finally, $Pt(dppe)_2$ shows a tetrahedral structure as expected for a zerovalent $Pt(LL)_2$ complex (Figure 12).[47,48]

3. CONCLUSIONS

A competition between the nonredox substitution with retention of the nuclearity and the redox fragmentation is observed in the case of the reactions of $[Pt_{3n}(CO)_{6n}]^{2-}$ Chini

DOI: 10.1021/acs.inorgchem.6b02750
Inorg. Chem. XXXX, XXX, XXX−XXX

Table 2. Main Bond Distances (Å) of $Pt_6(CO)_6(dppe)_3$ Compared to $Pt_6(CO)_6(dppe)_3$ and $[Pt_6(CO)_{12}]^{2-}$

	Pt−Pt intra-triangular	Pt−Pt inter-triangular	Pt−P
$Pt_6(CO)_6(dppe)_3$	2.6586(4)−2.6715(4) average 2.6667(10)	3.1110(4)−3.1589(4) average 3.1393(7)	2.2502(17)−2.2667(17) average 2.258(4)
$Pt_6(CO)_6(dppm)_3$ [a]	2.6427(5)−2.6945(5) average 2.6748(12)	3.0159(5)−3.1048(5) average 3.0567(9)	2.248(2)−2.273(2) average 2.260(5)
$[Pt_6(CO)_{12}]^{2-}$ [b]	2.644(7)−2.659(3) average 2.653(10)	3.026(16)−3.049(17) average 3.03(3)	

[a]From ref 43. [b]From ref 12.

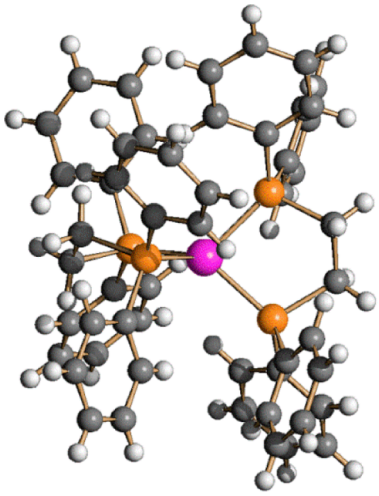

Figure 12. Molecular structure of $Pt(dppe)_2$ (Pt, purple; P, orange; C, gray, O, red).

clusters with phosphine ligands. The nonredox substitution results in heteroleptic analogues of anionic Chini clusters, whereas redox fragmentation (elimination) reactions afford lower nuclearity homoleptic species $[Pt_{3(n-1)}(CO)_{6(n-1)}]^{2-}$ as well as miscellaneous neutral complexes. In the case of the monodentate PPh_3 and bidentate dppe and R-dppp ligands, it has been possible to favor substitution over fragmentation by employing stoichiometric amounts of the ligands. Thus, the heteroleptic Chini clusters $[Pt_9(CO)_{16}(dppe)]^{2-}$, $[Pt_9(CO)_{16}(R\text{-dppp})]^{2-}$, $[Pt_6(CO)_{10}(dppe)]^{2-}$, and $[Pt_{12}(CO)_{20}(dppe)_2]^{2-}$ have been structurally characterized in this work, whereas the analogous PPh_3-derivatives $[Pt_{12}(CO)_{22}(PPh_3)_2]^{2-}$, $[Pt_9(CO)_{16}(PPh_3)_2]^{2-}$, and $[Pt_6(CO)_{10}(PPh_3)_2]^{2-}$ have been previously described.[36] Conversely, in the case of more rigid bidentate ligands, such as P^P, dppm, and dppb, it is not possible to isolate the substitution products, since fragmentation (elimination) proceeds very fast leading to neutral complexes.

The present work clearly demonstrates the possibility to functionalize anionic platinum Chini clusters and extend the scope of our previous work on monodentate ligands[36] also to bidentate and chiral phosphines. Heteroleptic and chiral Chini clusters might be in the future investigated for applications in catalysis.

Finally, from a structural point of view, the analysis of the structures of the heteroleptic anionic platinum Chini clusters so far characterized and their comparison to the homoleptic analogues, points out a high flexibility of the inter-triangular Pt−Pt interactions along the *pseudo*-C_3 axis. Indeed, while the triangular Pt_3 units are preserved in view of stronger intra-triangular Pt−Pt bonds, the overall trigonal prismatic structures present in the homoleptic clusters are readily deformed and transformed upon functionalization. Such transformations, which are due to both steric and electronic effects, may be just local deformations, as found in $[Pt_9(CO)_{16}(dppe)]^{2-}$, $[Pt_9(CO)_{16}(R\text{-dppp})]^{2-}$, $[Pt_{12}(CO)_{22}(PPh_3)_2]^{2-}$, and $[Pt_9(CO)_{16}(PPh_3)_2]^{2-}$; an inversion of the cage from trigonal prismatic to octahedral, as observed in $[Pt_6(CO)_{10}(dppe)]^{2-}$ and $[Pt_6(CO)_{10}(PPh_3)_2]^{2-}$; the reciprocal rotation of two trigonal prismatic units with the loss of a Pt−Pt contact as found in $[Pt_{12}(CO)_{20}(dppe)_2]^{2-}$. The latter structure is remarkable, since it may be viewed as a dimer composed of two mono-anionic $[Pt_6(CO)_{10}(dppe)]^-$ units joined by two (and not three) Pt−Pt interactions. Mono-anionic radicals of the type $[Pt_{3n}(CO)_{6n}]^-$ are sought to be intermediates in the oxidation of homoleptic Chini clusters,[49] and the present findings give some experimental support to this. In this respect, a mono-anionic $[Pt_3(\mu\text{-}CO)_3(CNR)_3]^-$ (R = 2,6-(2,6-(*i*-Pr)$_2C_6H_3)_2C_6H_3$) cluster with terminal isocyanide ligands was recently fully charactreized.[6] Overall, it seems that, 40 years since their discovery, platinum Chini clusters still display a rather rich and fascinating chemistry.

4. EXPERIMENTAL SECTION

4.1. General Procedures. All reactions and sample manipulations were performed using standard Schlenk techniques under nitrogen and in dried solvents. All the reagents were commercial products (Aldrich) of the highest purity available and used as received, except $[NEt_4]_2[Pt_9(CO)_{18}]$, $[NMe_3(CH_2Ph)]_2[Pt_{12}(CO)_{24}]$, $[NMe_4]_2[Pt_{12}(CO)_{24}]$, $[NEt_4]_2[Pt_6(CO)_{12}]$, and $[NMe_4]_2[Pt_6(CO)_{12}]$, which were prepared according to the literature.[1,2] Analysis of Pt was performed by atomic absorption on a Pye-Unicam instrument. Analyses of C, H, and N were obtained with a Thermo Quest Flash EA 1112NC instrument. IR spectra were recorded on a PerkinElmer Spectrum One interferometer in CaF_2 cells. $^{31}P\{^1H\}$ NMR measurements were performed on a Varian Mercury Plus 400 MHz instrument. The phosphorus chemical shifts were referenced to external H_3PO_4 (85% in D_2O). $^{31}P\{^1H\}$ NMR spectra were simulated with gNMR 5.0.6.0, using the experimental parameters (δ, J).[42] Structure drawings were performed with *SCHAKAL99*.[50]

4.2. Synthesis of $[NEt_4]_2[Pt_9(CO)_{16}(dppe)]\cdot 2CH_3COCH_3$. dppe (0.115 g, 0.289 mmol) was added as a solid to a solution of $[NEt_4]_2[Pt_9(CO)_{18}]$ (0.520 g, 0.206 mmol) in acetone (15 mL). The resulting mixture was stirred at room temperature for 2 h, and then, the solvent was removed in vacuo. The residue was washed with water (20 mL), toluene* (15 mL), and CH_2Cl_2 (15 mL) and extracted with acetone (15 mL). Crystals of $[NEt_4]_2[Pt_9(CO)_{16}(dppe)]\cdot 2CH_3COCH_3$ suitable for X-ray analyses were obtained by layering *n*-hexane (30 mL) on the acetone solution (yield 0.31 g, 51% based on Pt).

$C_{64}H_{76}N_2O_{18}P_2Pt_9$ (2979.02): calcd. C 25.80, H 2.57, N 0.94, Pt 58.94; found: C 26.02, H 2.78, N 0.79, Pt 59.13%. IR (nujol, 293 K) ν(CO): 2047(w), 2015(vs), 1997(sh), 1858(w), 1831(m), 1820(m),

DOI: 10.1021/acs.inorgchem.6b02750
Inorg. Chem. XXXX, XXX, XXX−XXX

Table 3. Crystal Data and Experimental Details for $[NMe_4]_2[Pt_6(CO)_{10}(dppe)]$, $[NEt_4]_2[Pt_6(CO)_{10}(dppe)]$, $[NEt_4]_2[Pt_9(CO)_{16}(dppe)]\cdot 2CH_3COCH_3$, $[NEt_4]_2[Pt_9(CO)_{16}(R\text{-}dppp)]\cdot 2CH_3COCH_3$, $[NMe_3(CH_2Ph)]_2[Pt_{12}(CO)_{20}(dppe)_2]\cdot CH_3CN$, $[NMe_4]_2[Pt_{12}(CO)_{20}(dppe)_2]\cdot 2CH_3CN$, $[Pt(dppe)_2][Pt_{12}(CO)_{24}]\cdot 2DMF$, $Pt(dppe)_2\cdot CH_2Cl_2$, $Pt_6(CO)_6(dppe)_3\cdot 3CH_2Cl_2$, and $Pt_4(CO)_4(dppe)_2\cdot 2THF$

	$[NMe_4]_2[Pt_6(CO)_{10}(dppe)]$	$[NEt_4]_2[Pt_6(CO)_{10}(dppe)]$	$[NEt_4]_2[Pt_9(CO)_{16}(dppe)]\cdot 2CH_3COCH_3$	$[NMe_3(CH_2Ph)]_2[Pt_{12}(CO)_{20}(dppe)_2]\cdot CH_3CN$
formula	$C_{44}H_{48}N_2O_{10}P_2Pt_6$	$C_{52}H_{64}N_2O_{10}P_2Pt_6$	$C_{64}H_{76}N_2O_{18}P_2Pt_9$	$C_{94}H_{83}N_3O_{20}P_4Pt_{12}$
Fw	1997.32	2109.53	2979.02	4039.59
T, K	100(2)	100(2)	291(2)	100(2)
λ, Å	0.710 73	0.710 73	0.710 73	0.710 73
crystal system	monoclinic	monoclinic	orthorhombic	triclinic
space group	$C2/c$	$C2/c$	$Pna2_1$	$P\bar{1}$
a, Å	22.7406(8)	25.2580(7)	29.341(6)	13.4798(5)
b, Å	11.3119(4)	11.2170(3)	14.916(3)	13.9719(6)
c, Å	22.0638(8)	21.8096(6)	17.883(4)	14.6962(6)
α, deg	90	90	90	95.293(2)
β, deg	120.489(2)	116.1000(10)	90	104.089(2)
γ, deg	90	90	90	112.579(2)
cell volume, Å^3	4890.9(3)	5549.0(3)	7826(3)	2424.94(17)
Z	4	4	4	1
D_c, g cm^{-3}	2.713	2.525	2.528	2.766
μ, mm^{-1}	17.217	15.183	16.121	17.365
$F(000)$	3616	3872	5400	1824
crystal size, mm	0.15 × 0.13 × 0.10	0.15 × 0.13 × 0.11	0.21 × 0.16 × 0.13	0.15 × 0.12 × 0.09
θ limits, deg	2.08−27.00	1.80−25.02	1.39−25.03	1.46−26.51
index ranges	$-28 \le h \le 28$	$-30 \le h \le 30$	$-34 \le h \le 33$	$-16 \le h \le 16$
	$-14 \le k \le 14$	$-13 \le k \le 13$	$-17 \le k \le 17$	$-17 \le k \le 17$
	$-28 \le l \le 28$	$-25 \le l \le 25$	$-21 \le l \le 21$	$-18 \le l \le 18$
reflections collected	40 003	38 717	72 956	38 438
independent reflections	5351 [R_{int} = 0.0511]	4906 [R_{int} = 0.0953]	13 712 [R_{int} = 0.0703]	9972 [R_{int} = 0.0651]
completeness to θ max	100.0%	99.9%	99.6%	98.9%
data/restraints/parameters	5351/30/289	4906/12/325	13 712/450/768	9972/299/538
goodness on fit on F^2	1.102	1.119	1.025	1.053
R_1 ($I > 2\sigma(I)$)	0.0218	0.0479	0.0392	0.0508
wR_2 (all data)	0.0451	0.1261	0.0850	0.1625
largest diff. peak and hole, e Å^{-3}	1.069/−1.394	4.217/−1.900	0.970/−1.351	2.965/−3.266

	$[NMe_4]_2[Pt_{12}(CO)_{20}(dppe)_2]\cdot 2CH_3CN$	$[Pt(dppe)_2][Pt_{12}(CO)_{24}]\cdot 2DMF$	$Pt_4(CO)_4(dppe)_2\cdot 2THF$
formula	$C_{84}H_{78}N_4O_{20}P_4Pt_{12}$	$C_{82}H_{62}N_2O_{26}P_4Pt_{13}$	$C_{64}H_{64}O_6P_4Pt_4$
Fw	3928.46	4151.39	1833.39
T, K	100(2)	100(2)	100(2)
λ, Å	0.710 73	0.710 73	0.710 73
crystal system	triclinic	monoclinic	triclinic
space group	$P\bar{1}$	Cc	$P\bar{1}$
a, Å	13.3433(4)	12.8023(2)	13.2249(2)
b, Å	13.8993(4)	34.8688(6)	13.4846(2)
c, Å	14.5522(4)	20.7130(4)	18.7808(3)
α, deg	95.896(2)	90	79.9740(10)
β, deg	103.899(2)	98.8280(10)	71.7440(10)
γ, deg	113.0710(10)	90	67.4040(10)
cell volume, Å^3	2351.04(12)	9136.8(3)	2930.97(8)
Z	1	4	2
D_c, g cm^{-3}	2.775	3.018	2.077
μ, mm^{-1}	17.906	19.959	9.677
$F(000)$	1766	7400	1736
crystal size, mm	0.16 × 0.13 × 0.12	0.16 × 0.12 × 0.10	0.15 × 0.12 × 0.10
θ limits, deg	1.48−26.00	1.53−26.00	1.64−27.00
index ranges	$-16 \le h \le 16$	$-15 \le h \le 15$	$-16 \le h \le 163$
	$-17 \le k \le 17$	$-42 \le k \le 42$	$-17 \le k \le 17$
	$-17 \le l \le 17$	$-25 \le l \le 25$	$-23 \le l \le 23$
reflections collected	36 872	71 622	49 701
independent reflections	9212 [R_{int} = 0.0677]	17 911 [R_{int} = 0.0552]	12 703 [R_{int} = 0.0556]
completeness to θ max	99.6%	100.0%	99.3%

DOI: 10.1021/acs.inorgchem.6b02750
Inorg. Chem. XXXX, XXX, XXX−XXX

Table 3. continued

	$[NMe_4]_2[Pt_{12}(CO)_{20}(dppe)_2]\cdot 2CH_3CN$	$[Pt(dppe)_2][Pt_{12}(CO)_{24}]\cdot 2DMF$	$Pt_4(CO)_4(dppe)_2\cdot 2THF$
data/restraints/parameters	9212/444/603	17 911/32/1145	12 703/184/749
goodness on fit on F^2	1.047	1.019	1.023
R_1 ($I > 2\sigma(I)$)	0.0355	0.0273	0.0318
wR_2 (all data)	0.0826	0.0625	0.0699
largest diff. peak and hole, e Å^{-3}	2.052/−2.418	1.713/−1.575	1.408/−1.654
	$[NEt_4]_2[Pt_9(CO)_{16}(R\text{-}dppp)_2]\cdot 2CH_3COCH_3$	$Pt(dppe)_2\cdot CH_2Cl_2$	$Pt_6(CO)_6(dppe)_3\cdot 3CH_2Cl_2$
formula	$C_{65}H_{78}N_2O_{18}P_2Pt_9$	$C_{53}H_{50}Cl_2P_4Pt$	$C_{87}H_{78}Cl_6O_6P_6Pt_6$
Fw	2993.04	1076.80	2788.55
T, K	100(2)	100(2)	100(2)
λ, Å	0.710 73	0.710 73	0.710 73
crystal system	monoclinic	monoclinic	triclinic
space group	$P2_1$	$P2_1/n$	$P\bar{1}$
a, Å	14.6912(9)	9.9225(4)	15.3436(5)
b, Å	17.7718(11)	20.8279(9)	15.7219(6)
c, Å	14.7316(9)	22.0699(9)	18.4766(7)
α, deg	90	90	92.720(2)
β, deg	94.221(4)	90.396(2)	98.368(2)
γ, deg	90	90	98.969(2)
cell volume, Å^3	3835.8(4)	4561.0(3)	4344.5(3)
Z	2	4	2
D_c, g cm^{-3}	2.591	1.568	2.132
μ, mm^{-1}	16.447	3.371	9.970
$F(000)$	2716	2160	2616
crystal size, mm	0.19 × 0.16 × 0.11	0.22 × 0.15 × 0.13	0.16 × 0.13 × 0.12
θ limits, deg	1.39−25.10	1.85−28.00	1.36−27.00
index ranges	$-17 \le h \le 17$	$-12 \le h \le 13$	$-19 \le h \le 19$
	$-21 \le k \le 21$	$-27 \le k \le 27$	$-20 \le k \le 20$
	$-17 \le l \le 17$	$-29 \le l \le 29$	$-23 \le l \le 23$
reflections collected	38 838	80 477	73 574
independent reflections	13 605 [R_{int} = 0.0899]	10 975 [R_{int} = 0.0669]	18 871 [R_{int} = 0.0747]
completeness to θ max	99.8%	99.8%	99.3%
data/restraints/parameters	13 605/505/876	10 975/0/541	18 871/0/1000
goodness on fit on F^2	0.989	1.018	1.017
R_1 ($I > 2\sigma(I)$)	0.0566	0.0280	0.0377
wR_2 (all data)	0.1560	0.0726	0.0870
largest diff. peak and hole, e Å^{-3}	3.952/−2.651	1.368/−1.754	3.530/−2.626

1804(ms) cm^{-1}. IR (acetone, 293 K) ν(CO): 2013(vs), 1831(ms) cm^{-1}. $^{31}P\{^1H\}$ NMR (CD_3CN, 298 K) δ (ppm): 48.1 ($^1J_{PtP}$ = 5060 Hz (1Pt), $^2J_{PtP}$ = 521 Hz (2Pt) and 17 Hz (1Pt), $^3J_{PP}$ = 8 Hz), 41.6 ($^1J_{PtP}$ = 4995 Hz (1Pt), $^2J_{PtP}$ = 632 Hz (2Pt) and 9 Hz (1Pt), $^3J_{PP}$ = 8 Hz).

*The toluene washing was dried in vacuo, and the residue was dissolved in THF (10 mL). Slow diffusion of *n*-hexane (25 mL) on the THF solution afforded a few crystals of $Pt_4(CO)_4(dppe)_2\cdot 2THF$ suitable for X-ray analyses. IR (nujol, 293 K) ν(CO): 1978(s), 1952(m) cm^{-1}.

4.3. Synthesis of $[NMe_3(CH_2Ph)]_2[Pt_{12}(CO)_{20}(dppe)_2]\cdot CH_3CN$. dppe (0.088 g, 0.221 mmol) was added as a solid to a solution of $[NMe_3(CH_2Ph)]_2[Pt_{12}(CO)_{24}]$ (0.350 g, 0.106 mmol) in acetone (15 mL). The resulting mixture was stirred at room temperature for 2 h, and then, the solvent was removed in vacuo. The residue was washed with CH_2Cl_2* (15 mL) and extracted with CH_3CN (15 mL). Crystals of $[NMe_3(CH_2Ph)]_2[Pt_{12}(CO)_{20}(dppe)_2]\cdot CH_3CN$ suitable for X-ray analyses were obtained by layering *n*-hexane (3 mL) and diisopropyl ether (30 mL) on the CH_3CN solution (yield 0.19 g, 44% based on Pt).

$C_{94}H_{83}N_3O_{20}P_4Pt_{12}$ (4039.59): calcd. C 27.94, H 2.07, N 1.04, Pt 57.95; found: C 27.76, H 2.21, N0.88, Pt 58.12%. IR (nujol, 293 K) ν(CO): 2008(vs), 1974(m), 1854(w), 1810(s) cm^{-1}. IR (acetone, 293 K) ν(CO): 2015(vs), 1854(w), 1832(s), 1810(m) cm^{-1}. IR (CH_3CN, 293 K) ν(CO): 2015(vs), 1854(w), 1828(s), 1807(m) cm^{-1}. IR (DMF, 293 K) ν(CO): 2012(vs), 1854(w), 1831(s), 1808(m) cm^{-1}. $^{31}P\{^1H\}$ NMR (DMF/CD_3CN, 298 K) δ (ppm): 47.7 ($^1J_{PtP}$ = 5024 Hz (1Pt), $^2J_{PtP}$ = 513 Hz (2Pt) and 19 Hz (1Pt), $^3J_{PP}$ = 8 Hz), 41.7 ($^1J_{PtP}$ = 5076 Hz (1Pt), $^2J_{PtP}$ = 528 Hz (2Pt) and 17 Hz (1Pt), $^3J_{PP}$ = 8 Hz).

$[NMe_4]_2[Pt_{12}(CO)_{20}(dppe)_2]\cdot 2CH_3CN$ was obtained employing a similar procedure starting from $[NMe_4]_2[Pt_{12}(CO)_{24}]$.

*Slow diffusion of *n*-hexane (25 mL) on the CH_2Cl_2 washing afforded a few crystals of $Pt_6(CO)_6(dppe)_3\cdot 3CH_2Cl_2$ suitable for X-ray analyses. IR (nujol, 293 K) ν(CO): 1792(vs) cm^{-1}. IR (CH_2Cl_2, 293 K) ν(CO): 1794(vs) cm^{-1}. $^{31}P\{^1H\}$ NMR (CD_2Cl_2, 298 K) δ (ppm): 52.1 ($^1J_{PtP}$ = 4825 Hz (1Pt), $^2J_{PtP}$ = 527 Hz (2Pt), $^3J_{PP}$ = 62 Hz (2P)).

4.4. Synthesis of $[NEt_4]_2[Pt_6(CO)_{10}(dppe)]$. dppe (0.238 g, 0.597 mmol) was added as a solid to a solution of $[NEt_4]_2[Pt_6(CO)_{12}]$ (0.480 g, 0.272 mmol) in CH_3CN (15 mL). The resulting mixture was stirred at room temperature for 2 h, and then, the solvent was removed in vacuo. The residue was washed with toluene* (15 mL) and CH_2Cl_2 (15 mL) and extracted with DMF (15 mL). Crystals of $[NEt_4]_2[Pt_6(CO)_{10}(dppe)]$ suitable for X-ray analyses were obtained by layering isopropanol (30 mL) on the DMF solution (yield 0.26 g, 45% based on Pt).

$C_{52}H_{64}N_2O_{10}P_2Pt_6$ (2109.53): calcd. C 29.60, H 3.06, N 1.33, Pt 55.49; found: C 29.41, H 2.84, N 1.52, Pt 55.22%. IR (nujol, 293 K) ν(CO): 1975(s), 1955(vs), 1756(s), 1732(ms) cm^{-1}. IR (CH_3CN, 293 K) ν(CO): 1976(vs), 1784(s), 1765(s) cm^{-1}. $^{31}P\{^1H\}$ NMR (DMF/CD_3CN, 298 K) δ (ppm): 51.2 ($^1J_{PtP}$ = 5086 Hz (1Pt), $^2J_{PtP}$ = 550 Hz (2Pt) and 21 Hz (1Pt)).

DOI: 10.1021/acs.inorgchem.6b02750
Inorg. Chem. XXXX, XXX, XXX−XXX

$[NMe_4]_2[Pt_6(CO)_{10}(dppe)]$ was obtained employing a similar procedure starting from $[NMe_4]_2[Pt_6(CO)_{12}]$.

*The toluene washing was dried in vacuo, and the residue dissolved in CH_2Cl_2 (10 mL). Slow diffusion of *n*-hexane (25 mL) on the CH_2Cl_2 solution afforded a few crystals of $Pt(dppe)_2{\cdot}CH_2Cl_2$ suitable for X-ray analyses. $^{31}P\{^1H\}$ NMR (CD_2Cl_2, 298 K) δ (ppm): 29.8 ($^1J_{Pt-P}$ = 3734 Hz).

4.5. Synthesis of $[NEt_4]_2[Pt_9(CO)_{16}(R\text{-dppp})]{\cdot}2CH_3COCH_3$. R-dppp (0.119 g, 0.289 mmol) was added as a solid to a solution of $[NEt_4]_2[Pt_9(CO)_{18}]$ (0.520 g, 0.206 mmol) in acetone (15 mL). The resulting mixture was stirred at room temperature for 2 h, and then, the solvent removed in vacuo. The residue was washed with toluene (15 mL) and extracted with acetone (15 mL). Crystals of $[NEt_4]_2[Pt_9(CO)_{16}(R\text{-dppp})]{\cdot}2CH_3COCH_3$ suitable for X-ray analyses were obtained by layering *n*-hexane (30 mL) on the acetone solution (yield 0.31 g, 51% based on Pt).

$C_{65}H_{78}N_2O_{18}P_2Pt_9$(2993.04): calcd. C 26.08, H 2.63, N 0.94, Pt 58.66; found: C 26.21, H 2.44, N 1.10, Pt 58.47%. IR (acetone, 293 K) ν(CO): 2014(vs), 1812(ms) cm^{-1}. $^{31}P\{^1H\}$ NMR (CD_3COCD_3, 298 K) δ (ppm) isomer I: 59.8 ($^1J_{PtP}$ = 5037 Hz (1Pt), $^2J_{PtP}$ = 517 Hz (2Pt), $^3J_{PP}$ = 11 Hz), 48.0 ($^1J_{PtP}$ = 4436 Hz (1Pt), $^2J_{PtP}$ = 529 Hz (2Pt), $^3J_{PP}$ = 11 Hz); isomer II: 51.2 ($^1J_{PtP}$ = 4944 Hz (1Pt), $^2J_{PtP}$ = 649 Hz (2Pt), $^3J_{PP}$ = 10 Hz), 41.2 ($^1J_{PtP}$ = 5033 Hz (1Pt), $^2J_{PtP}$ = 648 Hz (2Pt), $^3J_{PP}$ = 10 Hz).

4.6. X-ray Crystallographic Study. Crystal data and collection details for $[NMe_4]_2[Pt_6(CO)_{10}(dppe)]$, $[NEt_4]_2[Pt_6(CO)_{10}(dppe)]$, $[NEt_4]_2$ $[Pt_9(CO)_{16}(dppe)]{\cdot}2CH_3COCH_3$, $[NEt_4]_2[Pt_9(CO)_{16}(R\text{-dppp})]{\cdot}2CH_3COCH_3$, $[NMe_3(CH_2Ph)]_2$ $[Pt_{12}(CO)_{20}(dppe)_2]{\cdot}CH_3CN$, $[NMe_4]_2[Pt_{12}(CO)_{20}(dppe)_2]{\cdot}2CH_3CN$, $[Pt(dppe)_2]$-$[Pt_{12}(CO)_{24}]{\cdot}2DMF$, $Pt(dppe)_2{\cdot}CH_2Cl_2$, $Pt_6(CO)_6(dppe)_3{\cdot}3CH_2Cl_2$, and $Pt_4(CO)_4(dppe)_2{\cdot}2THF$ are reported in Table 3. The diffraction experiments were performed on a Bruker APEX II diffractometer equipped with a CCD detector using Mo Kα radiation. Data were corrected for Lorentz polarization and absorption effects (empirical absorption correction *SADABS*).[51] Structures were solved by direct methods and refined by full-matrix least-squares based on all data using F^2.[52] Hydrogen atoms were fixed at calculated positions and refined by a riding model. All non-hydrogen atoms were refined with anisotropic displacement parameters, unless otherwise stated. Among the 10 crystal structures herein reported, five do not show any alert of levels A or B in their checkcifs. Three structures present alerts of levels A and B, and two structures present alerts of level B. All the alerts of levels A and B are due to high values for the residual electron density. These maxima are located close to the Pt atoms, in positions that are not realistic for any atom, and they are series termination errors, which are common with heavy atoms such as Pt, especially in the case of high nuclearity clusters.

$[NMe_4]_2[Pt_6(CO)_{10}(dppe)]$. The asymmetric unit of the unit cell contains half of a cluster anion (located on 2) and one $[NMe_4]^+$ cation (located on a general position). Similar *U* restraints were applied to the $[NMe_4]^+$ cation (SIMU command in *SHELXL*, s.u. 0.01).

$[NEt_4]_2[Pt_6(CO)_{10}(dppe)]$. The asymmetric unit of the unit cell contains half of a cluster anion (located on 2) and one $[NEt_4]^+$ cation (located on a general position). One CO ligand was restrained to isotropic behavior (ISOR command in *SHELXL*, s.u. 0.01).

$[NEt_4]_2[Pt_9(CO)_{16}(dppe)]{\cdot}2CH_3COCH_3$. The asymmetric unit of the unit cell contains one cluster anion, two $[NEt_4]^+$ cations, and two CH_3COCH_3 molecules (all located on general positions). The CH_3COCH_3 molecules were refined isotropically. Some C and O atoms of the cluster anion were restrained to isotropic behavior (ISOR command in *SHELXL*, s.u. 0.04). The P and C atoms of the dppe ligands, the C and N atoms of the $[NEt_4]^+$ cations, and the C and O atoms of the CH_3COCH_3 molecules were restrained to have similar *U* parameters (SIMU command in *SHELXL*, s.u. 0.02). All the aromatic rings were constrained to fit regular hexagons (AFIX 66 command in *SHELXL*). The CH_3COCH_3 molecules were restrained to have similar geometries (SAME command in *SHELXL*, s.u. 0.02). Restraints to bond distances were applied as follows (s.u. 0.02): 1.47 Å for C−N and 1.53 Å for C−C in $[NEt_4]^+$; 1.21 Å for C−O and 1.51 Å for C−C in CH_3COCH_3.

$[NMe_3(CH_2Ph)]_2[Pt_{12}(CO)_{20}(dppe)_2]{\cdot}CH_3CN$. The asymmetric unit of the unit cell contains half of a cluster anion (located on $\bar{1}$), one $[NMe_3(CH_2Ph)]^+$ cation (located on a general position), and half of a CH_3CN molecule disordered over two symmetry related (by $\bar{1}$) positions. The CH_3CN molecule was refined isotropically. The C atoms of the dppe ligands, the C and N atoms of the $[NMe_3(CH_2Ph)]^+$ cations, and the C and N atoms of the CH_3CN molecule were restrained to have similar *U* parameters (SIMU command in *SHELXL*, s.u. 0.01). The $[NMe_3(CH_2Ph)]^+$ cations were restrained to isotropic behavior (ISOR command in *SHELXL*, s.u. 0.01). All the aromatic rings were constrained to fit regular hexagons (AFIX 66 command in *SHELXL*). Restraints to bond distances were applied as follows (s.u. 0.02): 1.47 Å for C−N and 1.51 Å for C−C in $[NMe_3(CH_2Ph)]^+$; 1.14 Å for C−N and 1.47 Å for C−C in CH_3CN.

$[NMe_4]_2[Pt_{12}(CO)_{20}(dppe)_2]{\cdot}2CH_3CN$. The asymmetric unit of the unit cell contains half of a cluster anion (located on $\bar{1}$), one $[NMe_4]^+$ cation (located on a general position), and two halves of two CH_3CN molecules disordered over symmetry related (by $\bar{1}$) positions. The C atoms of the dppe ligands, the C and N atoms of the $[NMe_4]^+$ cations, and the C and N atoms of the CH_3CN molecules were restrained to have similar *U* parameters (SIMU command in *SHELXL*, s.u. 0.02). All the aromatic rings were constrained to fit regular hexagons (AFIX 66 command in *SHELXL*). The $[NMe_4]^+$ cations were restrained to isotropic behavior (ISOR command in *SHELXL*, s.u. 0.02). Restraints to bond distances were applied as follows (s.u. 0.02): 1.14 Å for C−N and 1.47 Å for C−C in CH_3CN.

$[Pt(dppe)_2][Pt_{12}(CO)_{24}]{\cdot}2DMF$. The asymmetric unit of the unit cell contains one cluster anion, one $[Pt(dppe)_2]^{2+}$ cation, and two DMF molecules (all located on general positions). The crystals are racemically twinned with refined batch factor 0.513(6). The structure could not be solved in *C*2/*c*, and *Cc* is the correct space group, which gave the best refinement.

$Pt_4(CO)_4(dppe)_2{\cdot}2THF$. The asymmetric unit of the unit cell contains one cluster molecule and two THF molecules (all located on general positions). One THF molecule is disordered and was split into two positions and refined using one occupancy factor. The THF molecules were restrained to have similar geometries (SAME command in *SHELXL*, s.u. 0.02). The *U* parameters of the disordered THF molecule were restrained to be similar (SIMU command in *SHELXL*, s.u. 0.01). Restraints to bond distances were applied as follows (s.u. 0.01): 1.43 Å for C−O and 1.53 Å for C−C in the disordered THF molecule.

$[NEt_4]_2[Pt_9(CO)_{16}(R\text{-dppp})]{\cdot}2CH_3COCH_3$. The asymmetric unit of the unit cell contains one cluster anion, two $[NEt_4]^+$ cations, and two CH_3COCH_3 molecules (all located on general positions). The cluster anion is actually a mixture of two isomers because of the disorder of the Me group, which can be found bonded to C(61) or C(62) in ca. a 1:1 ratio. Some C and O atoms of the cluster anion and C atoms of the cations were restrained to isotropic behavior (ISOR command in *SHELXL*, s.u. 0.01). The *U* parameters of the R-dppp ligand, $[NEt_4]^+$ cations, and CH_3COCH_3 molecules were restrained to be similar (SIMU command in *SHELXL*, s.u. 0.02).

$Pt(dppe)_2{\cdot}CH_2Cl_2$. The asymmetric unit of the unit cell contains one cluster molecule and one CH_2Cl_2 molecule (all located on general positions).

$Pt_6(CO)_6(dppe)_3{\cdot}3CH_2Cl_2$. The asymmetric unit of the unit cell contains one cluster molecule and three CH_2Cl_2 molecules (all located on general positions).

■ ASSOCIATED CONTENT

Supporting Information

The Supporting Information is available free of charge on the ACS Publications website at DOI: 10.1021/acs.inorgchem.6b02750.

Comparison of the experimental and simulated ^{31}P NMR spectra of $[Pt_9(CO)_{16}(dppe)]^{2-}$, $Pt_6(CO)_6(dppe)_3$, $Pt(dppe)_2$, $[Pt_{12}(CO)_{20}(dppe)_2]^{2-}$, $[Pt_6(CO)_{10}(dppe)]^{2-}$, $[Pt_9(CO)_{16}(R\text{-dppp})]^{2-}$, $[Pt_6(CO)_{10}(R\text{-dppp})]^{2-}$. Mo-

DOI: 10.1021/acs.inorgchem.6b02750
Inorg. Chem. XXXX, XXX, XXX−XXX

lecular structure of $[Pt(dppe)_2][Pt_{12}(CO)_{24}]\cdot 2DMF$ (PDF)
Crystallographic data in CIF format (CIF)

■ AUTHOR INFORMATION

Corresponding Author

*E-mail: stefano.zacchini@unibo.it.

ORCID

Stefano Zacchini: 0000-0003-0739-0518

Notes

The authors declare no competing financial interest.

■ ACKNOWLEDGMENTS

The Univ. of Bologna is acknowledged for financial support of this work (FARB–Linea d'Intervento 2, "Catalytic transformation of biomass-derived materials into high added-value chemicals", 2014-2016).

■ REFERENCES

(1) Longoni, G.; Chini, P. Synthesis and chemical characterization of platinum carbonyl dianions $[Pt_3(CO)_6]_n^{2-}$ (n = ∼ 10, 6, 5, 4, 3, 2, 1). A new series of inorganic oligomers. *J. Am. Chem. Soc.* **1976**, *98*, 7225.

(2) Calabrese, J. C.; Dahl, L. F.; Chini, P.; Longoni, G.; Martinengo, S. Synthesis and structural characterization of platinum carbonyl dianions, $[Pt_3(CO)_3(\mu\text{-}CO)_3]_n^{2-}$ (n = 1, 3, 4, 5). A new series of inorganic oligomers. *J. Am. Chem. Soc.* **1974**, *96*, 2614.

(3) Ciabatti, I.; Femoni, C.; Iapalucci, M. C.; Longoni, G.; Zacchini, S. Platinum Carbonyl Clusters Chemistry: Four Decades of Challenging Nanoscience. *J. Cluster Sci.* **2014**, *25*, 115.

(4) Gao, F.; Li, C.; Heaton, B. T.; Zacchini, S.; Zarra, S.; Longoni, G.; Garland, M. The inter-conversions of platinum carbonyl dianionic clusters, $[Pt_3(CO)_6]_n^{2-}$ (n = 2−5), in THF and acetonitrile. A combined in situ FTIR spectroscopic and BTEM study leading to the characterization of the new $[H_{4-x}Pt_{15}(CO)_{19}]^{x-}$ (x = 2−4) clusters. *Dalton Trans.* **2011**, *40*, 5002.

(5) (a) Ceriotti, A.; Longoni, G.; Marchionna, M. Bis(tetrabutylammonium) hexa-μ-carbonyl-hexacarbonylhexaplatinate(2-), $[N(C_4H_9)_4]_2[Pt_6(CO)_6(\mu\text{-}CO)_6]$. *Inorganic Syntheses* **1989**, *26*, 316. (b) Brown, C.; Heaton, B. T.; Chini, P.; Fumagalli, A.; Longoni, G. Stereochemical non-rigidity of a metal polyhedron: Fourier transform platinum-195 nuclear magnetic resonance spectra of $[Pt_n(CO)_{2n}]^{2-}$ (n = 3, 6, or 9). *J. Chem. Soc., Chem. Commun.* **1977**, 309. (c) Brown, C.; Heaton, B. T.; Towl, A. D. C.; Fumagalli, A.; Longoni, G.; et al. Stereochemical non-rigidity of a metal polyhedron: carbon-13 and platinum-195 Fourier transform nuclear magnetic resonance spectra of $[Pt_n(CO)_{2n}]^{2-}$ (n = 3, 6, 9, 12 or 15). *J. Organomet. Chem.* **1979**, *181*, 233.

(6) Barnett, B. R.; Rheingold, A. L.; Figueroa, J. S. Monomeric Chini-Type Triplatinum Clusters Featuring Dianionic and Radical-Anionic π^*-Systems. *Angew. Chem., Int. Ed.* **2016**, *55*, 9253.

(7) (a) Femoni, C.; Kaswalder, F.; Iapalucci, M. C.; Longoni, G.; Mehlstäubl, M.; Zacchini, S. High-yield one-step synthesis in water of $[Pt_{3n}(CO)_{6n}]^{2-}$ ($n > 6$) and $[Pt_{38}(CO)_{44}]^{2-}$. *Chem. Commun.* **2005**, 5769. (b) Femoni, C.; Kaswalder, F.; Iapalucci, M. C.; Longoni, G.; Mehlstäubl, M.; Zacchini, S.; Ceriotti, A. Synthesis and Crystal Structure of $[NBu_4]_2[Pt_{24}(CO)_{48}]$: An Infinite 1D Stack of $\{Pt_3(CO)_6\}$ Units Morphologically Resembling a CO-Insulated Platinum Cable. *Angew. Chem., Int. Ed.* **2006**, *45*, 2060.

(8) (a) Femoni, C.; Kaswalder, F.; Iapalucci, M. C.; Longoni, G.; Zacchini, S. Infinite Molecular $\{[Pt_{3n}(CO)_{6n}]^{2-}\}_\infty$ Conductor Wires by Self-Assembly of $[Pt_{3n}(CO)_{6n}]^{2-}$ (n = 5−8) Cluster Dianions Formally Resembling CO-Sheathed Three-Platinum Cables. *Eur. J. Inorg. Chem.* **2007**, *2007*, 1483. (b) Femoni, C.; Iapalucci, M. C.; Longoni, G.; Lovato, T.; Stagni, S.; Zacchini, S. Self-Assembly of $[Pt_{3n}(CO)_{6n}]^{2-}$ (n = 4−8) Carbonyl Clusters: from Molecules to Conducting Molecular Metal Wires. *Inorg. Chem.* **2010**, *49*, 5992.

(9) Greco, P.; Cavallini, M.; Stoliar, P.; Quiroga, S. D.; Dutta, S.; Zacchini, S.; Iapalucci, M. C.; Morandi, V.; Milita, S.; Merli, P. G.; Biscarini, F. Conductive Sub-micrometric Wires of Platinum-Carbonyl Clusters Fabricated by Soft-Lithography. *J. Am. Chem. Soc.* **2008**, *130*, 1177.

(10) Serban, D. A.; Greco, P.; Melinte, S.; Vlad, A.; Dutu, C. A.; Zacchini, S.; Iapalucci, M. C.; Biscarini, F.; Cavallini, M. Towards All-Organic Field-Effect Transistors by Additive Soft Lithography. *Small* **2009**, *5*, 1117.

(11) (a) Zacchini, S. Using Metal Carbonyl Clusters To Develop a Molecular Approach towards Metal Nanoparticles. *Eur. J. Inorg. Chem.* **2011**, *2011*, 4125. (b) Femoni, C.; Iapalucci, M. C.; Kaswalder, F.; Longoni, G.; Zacchini, S. The possible role of metal carbonyl clusters in nanoscience and nanotechnologies. *Coord. Chem. Rev.* **2006**, *250*, 1580.

(12) (a) Ichikawa, M. Specific dehydrocyclisation of n-hexane over supported platinum crystallites prepared from platinum carbonyl cluster anion salts. *J. Chem. Soc., Chem. Commun.* **1976**, 11. (b) Sasaki, M.; Osada, M.; Higashimoto, N.; Yamamoto, T.; Fukuoka, A.; Ichikawa, M. Templating fabrication of platinum nanoparticles and nanowires using the confined mesoporous channels of FSM-16. Their structural characterization and catalytic performances in water gas shift reaction. *J. Mol. Catal. A: Chem.* **1999**, *141*, 223. (c) Ichikawa, M. "Ship-in-Bottle" Catalyst Technology: Novel Templating Fabrication of Platinum Group Metals Nanoparticles and Wires in Micro/Mesopores. *Platinum Met. Rev.* **2000**, *44*, 3. (d) Fukuoka, A.; Higashimoto, N.; Sakamoto, Y.; Sasaki, M.; Sugimoto, N.; Inagaki, S.; Fukushima, Y.; Ichikawa, M. Ship-in bottle synthesis and catalytic performances of platinum carbonyl clusters, nanowires, and nanoparticles in micro- and mesoporous materials. *Catal. Today* **2001**, *66*, 23.

(13) (a) Maity, P.; Basu, S.; Bhaduri, S.; Lahiri, G. K. Superior performance of a nanostructured platinum catalyst in water: Hyrogenations of alkanes, aldehydes and nitroaromatics. *Adv. Synth. Catal.* **2007**, *349*, 1955. (b) Bhaduri, S.; Lahiri, G. K.; Munshi, P.; Mukesh, D. Asymmetric hydrogenation of methyl pyruvate using platinum carbonyl cluster supported on an anion exchanger as the catalyst. *Catal. Lett.* **2000**, *65*, 61. (c) Maity, P.; Gopinath, C. S.; Bhaduri, S.; Lahiri, G. K. Applications of a high performance platinum nanocatalyst for the oxidation of alcohols in water. *Green Chem.* **2009**, *11*, 554. (d) Maity, P.; Basu, S.; Bhaduri; Lahiri, G. K. A water soluble nanostructured platinum(0) metal catalyst from platinum carbonyl molecular clusters: Synthesis, characterization and application in the selective hydrogenations of olefins, ketones and aldehydes. *J. Mol. Catal. A: Chem.* **2007**, *270*, 117.

(14) (a) Bhaduri, S. Catalysis with platinum carbonyl clusters. *Curr. Sci.* **2000**, *78*, 1318. (b) Sen Gupta, N.; Basu, S.; Payra, P.; Mathur, P.; Bhaduri, S.; Lahiri, G. K. Reduction of nitrite to NO in an organized triphasic medium by platinum carbonyl clusters and redox active dyes as electron carries. *Dalton Trans.* **2007**, 2594. (c) Paul, H.; Basu, S.; Bhaduri, S.; Lahiri, G. K. Platinum carbonyl derived catalysts on inorganic and organic supports: A comparative study. *J. Organomet. Chem.* **2004**, *689*, 309.

(15) (a) Le Gratiet, B.; Remita, H.; Picq, G.; Delcourt, M. O. CO-stabilized supported Pt catalysts for fuel cells: Radiolytic synthesis. *J. Catal.* **1996**, *164*, 36. (b) Kowalska, E.; Remita, H.; Colbeau-Justin, C.; Hupka, J.; Belloni, J. Modification of titanium dioxide with platinum ions and clusters: Application in photocatalysis. *J. Phys. Chem. C* **2008**, *112*, 1124. (c) Remita, H.; Keita, B.; Torigoe, K.; Belloni, J.; Nadjo, L. Platinum nanowires and layers obtained by self-assembly of Chini clusters deposited on supports. *Surf. Sci.* **2004**, *572*, 301. (d) Henglein, F. A. Formation of a Pt-carbonyl colloid by reaction of colloidal Pt with CO. *J. Phys. Chem. B* **1997**, *101*, 5889.

(16) (a) Chang, J.-R.; Koningsberger, D. C.; Gates, B. C. Structurally simple supported platinum clusters prepared from $[Pt_{15}(CO)_{30}]^{2-}$ on magnesium oxide. *J. Am. Chem. Soc.* **1992**, *114*, 6460. (b) Chen, G.; Yang, H.; Wu, B.; Zheng, Y.; Zheng, N. Supported monodisperse Pt nanoparticles from $[Pt_3(CO)_3(\mu_2\text{-}CO)_3]_5^{2-}$ clusters for investigating supports-Pt interface effect in catalysis. *Dalton Trans.* **2013**, *42*, 12699.

DOI: 10.1021/acs.inorgchem.6b02750
Inorg. Chem. XXXX, XXX, XXX−XXX

(c) Drozdová, L.; Brabec, L.; Nováková, J.; Beneke, M.; Jaeger, N.; Schulz-Ekloff, G. Subnanometer platinum clusters in zeolite NaEMT via stoichiometric carbonyl clusters. *Microporous Mesoporous Mater.* **2000**, *35−36*, 511. (d) Kubelková, L.; Drozdová, L.; Brabec, L.; Nováková, J.; Kotrla; Hulstede, P.; Jaeger, N.; Schulz-Ekloff, G. Anionic Pt carbonyl complexes in faujasites: Matrix effect. *J. Phys. Chem.* **1996**, *100*, 15517.

(17) (a) Lewis, G. J.; Roth, J. D.; Montag, R. A.; Safford, L. K.; Gao, X.; Chang, S.-C.; Dahl, L. F.; Weaver, M. J. Electroactive metal-clusters as models of electrode surfaces. vibrational spectroelectrochemistry of 7 redox forms of $[Pt_{24}(CO)_{30}]^n$ (n = 0 to −6) and comparison with potential-dependent spectra of CO chemisorbed on platinum. *J. Am. Chem. Soc.* **1990**, *112*, 2831. (b) Roth, J. D.; Lewis, G. J.; Safford, L. K.; Jiang, X.; Dahl, L. F.; Weaver, M. J. Exploration of the ionizable metal cluster electrode surface analogy - infrared spectroelectrochemistry of $[Pt_{24}(CO)_{30}]^n$, $[Pt_{26}(CO)_{32}]^n$, and $[Pt_{38}(CO)_{44}]^n$ (n = 0 to −10) and comparisons with potential-dependent spectra of CO adlayers on platinum surfaces. *J. Am. Chem. Soc.* **1992**, *114*, 6159.

(18) Fedi, S.; Zanello, P.; Laschi, F.; Ceriotti, A.; El Afefey, S. A joint electrochemical/spectroelectrochemical inspection (and re-inspection) of high-nuclearity platinum carbonyl clusters. *J. Solid State Electrochem.* **2009**, *13*, 1497.

(19) Ceriotti, A.; Masciocchi, N.; Macchi, P.; Longoni, G. $[Pt_{19}(CO)_{21}(NO)]^{3-}$ and $[Pt_{38}(CO)_{44}]^{2-}$: nitrosyl bending through intramolecular electron transfer as an intermediate step in the nucleation process from polydecker to ccp platinum carbonyl clusters. *Angew. Chem., Int. Ed.* **1999**, *38*, 3724.

(20) Washecheck, D. M.; Wucherer, E. J.; Dahl, L. F.; Ceriotti, A.; Longoni, G.; Manassero, M.; Sansoni, M.; Chini, P. Synthesis, structure, and stereochemical implications of the $[Pt_{19}(CO)_{12}(\mu\text{-}CO)_{10}]^{4-}$ tetraanion: A bicapped triple-decker all-metal sandwich of idealized fivefold (D_{5h}) geometry. *J. Am. Chem. Soc.* **1979**, *101*, 6110.

(21) Cattabriga, E.; Ciabatti, I.; Femoni, C.; Funaioli, T.; Iapalucci, M. C.; Zacchini, S. Syntheses, Structures, and Electrochemistry of the Defetctive *ccp* $[Pt_{33}(CO)_{38}]^{2-}$ and the *bcc* $[Pt_{40}(CO)_{40}]^{6-}$ Molecular Nanoclusters. *Inorg. Chem.* **2016**, *55*, 6068.

(22) (a) Ciabatti, I.; Femoni, C.; Iapalucci, M. C.; Longoni, G.; Zacchini, S.; Zarra, S. Surface decorated platinum carbonyl clusters. *Nanoscale* **2012**, *4*, 4166. (b) Femoni, C.; Iapalucci, M. C.; Longoni, G.; Zacchini, S.; Zarra, S. Icosahedral Pt-Centered $Pt_{13}$and Pt_{19} Carbonyl Clusters Decorated by $[Cd_5(\mu\text{-}Br)_5Br_{5\text{-}x}(solvent)_x]^{x+}$ Rings Reminiscent of the Decoration of Au-Fe-CO and Au-Thiolate Nanoclusters: A Unifying Approach to Their Electron Counts. *J. Am. Chem. Soc.* **2011**, *133*, 2406.

(23) (a) Bortoluzzi, M.; Ceriotti, A.; Cesari, C.; Ciabatti, I.; Della Pergola, R.; Femoni, C.; Iapalucci, M. C.; Storione, A.; Zacchini, S. Syntheses of $[Pt_6(CO)_8(SnCl_2)\ (SnCl_3)_4]^{4-}$ and $[Pt_6(CO)_8(SnCl_2)(SnCl_3)_2(PPh_3)_2]^{2-}$ Platinum-Carbonyl Clusters Decorated by Sn^{II} Fragments. *Eur. J. Inorg. Chem.* **2016**, *2016*, 3939. (b) Bortoluzzi, M.; Ceriotti, A.; Ciabatti, I.; Della Pergola, R.; Femoni, C.; Iapalucci, M. C.; Storione, A.; Zacchini, S. Platinum carbonyl clusters stabilized by Sn(II)-based fragments: syntheses and structures of $[Pt_6(CO)_6(SnCl_2)_2(SnCl_3)_4]^{4-}$, $[Pt_9(CO)_8(SnCl_2)_3(SnCl_3)_2(Cl_2SnOCOSnCl_2)]^{4-}$ and $[Pt_{10}(CO)_{14}\{Cl_2Sn(OH)SnCl_2\}_2]^{2-}$. *Dalton Trans.* **2016**, *45*, 5001.

(24) (a) Brivio, E.; Ceriotti, A.; Garlaschelli, L.; Manassero, M.; Sansoni, M. Coordination of $SnCl_2$and $GeCl_2$ onto a one-dimensional platinum network - Synthesis and structural characterization of the $[PPh_4]_2[Pt_8(ECl_2)_4(CO)_{10}]$ (E = Sn, Ge) complexes. *J. Chem. Soc., Chem. Commun.* **1995**, 2055. (b) Ceriotti, A.; Daghetta, M.; El Afefey, S.; Ienco, A.; Longoni, G.; Manca, G.; Mealli, C.; Zacchini, S.; Zarra, S. Electronic Stabilization of Trigonal Bipyramidal Clusters: the Role of the Sn(II) Ions in $[Pt_5(CO)_5\{Cl_2Sn(\mu\text{-}OR)SnCl_2\}_3]^{3-}$ (R = H, Me, Et, ^{i}Pr). *Inorg. Chem.* **2011**, *50*, 12553.

(25) (a) *Clusters and Colloids;* Schmid, G., Ed.; Wiley-VCH: New York, 1994. (b) *Metal Clusters in Chemistry;* Braunstein, P., Oro, L. A., Raithby, P. R., Eds.; Wiley-VCH: New York, 1999.

(26) Vargas, M. D.; Nicholls, J. N. High-nuclearity carbonyl clusters - Their synthesis and reactivity. *Adv. Inorg. Chem.* **1986**, *30*, 123.

(27) Chini, P. Large metal carbonyl clusters (LMCC). *J. Organomet. Chem.* **1980**, *200*, 37.

(28) (a) *Catalysis by Di- and Polynuclear Metal Cluster Complexes;* Adams, R. D., Cotton, F. A., Eds; Wiley-VCH: New York, 1998. (b) *Metal Clusters in Catalysis;* Gates, B. C., Guczi, L., Knözinger, H., Eds.; Elsevier: Amsterdam, The Netherlands, 1986. (c) *The Chemistry of Metal Clusters Complexes;* Shriver, D. F., Kaesz, H. D., Adams, R. D., Eds.; VCH Publishers: New York, 1990.

(29) Adams, R. D.; Captain, B. Unusual structures and reactivity of mixed metal clusters complexes containing the palladium/platinum tri-t-butylphosphine grouping. *Acc. Chem. Res.* **2009**, *42*, 409.

(30) (a) Gourdon, A.; Jeannin, Y. The synthesis of phosphine derivatives of $[Fe_4N(CO)_{12}]^-$ - Crystal structures of $[Fe_4N(CO)_9(NO)\ (PPh_3)_2]$, $[HFe_4N(CO)_{11}(PPh_3)]$ and $[(PPh_3)_2N][Fe_4N(CO)_{11}(PMe_2PH)]$. *J. Organomet. Chem.* **1992**, *440*, 353. (b) Zanello, P.; Laschi, F.; Cinquantini, A.; Della Pergola, R.; Garlaschelli, L.; Cucco, M.; Demartin, F.; Spalding, T. R. The redox behavior of the cluster anion $[Fe_4N(CO)_{12}]^-$. Electron-transfer chain catalytic substitution-reactions, crystal structure of $[Fe_4N(CO)_{11}(PPh_3)]^-$. *Inorg. Chim. Acta* **1994**, *226*, 1.

(31) (a) Blum, T.; Brown, M. P.; Heaton, B. T.; Hor, A. S.; Iggo, J. A.; Sabounchei, J. S. Z.; Smith, A. K. Phosphine-substituted trigonal-prismatic and octahedral clusters. *J. Chem. Soc., Dalton Trans.* **1994**, 513. (b) Sabounchei, J. S. Z.; Heaton, B. T.; Iggo, J. A.; Jacob, C.; Podkorytov, I. S. 1- and 2-D NMR studies on $[Rh_6C(CO)_{14}(PPh_3)]^{2-}$. *J. Cluster Sci.* **2001**, *12*, 339.

(32) (a) Bordoni, S.; Heaton, B. T.; Seregni, C.; Strona, L.; Goodfellow, R. J.; Hursthouse, M. B.; Thornton-Pett, M.; Martinengo, S. Derivatives of $[Rh_6(CO)_{13}C]^{2-}$ - Solution structure of $[Rh_6H(CO)_{13}C]^-$ from nuclear magnetic resonance measurements and the X-ray crystal structure of $[Rh_6(CO)_{11}C(\mu\text{-}Ph_2PCH_2CH_2PPh_2)]^{2-}$. *J. Chem. Soc., Dalton Trans.* **1988**, 2103. (b) Della Pergola, R.; Garlaschelli, L.; Manassero, M.; Sansoni, M.; Strumolo, D. Iridium cluster chemistry: The synthesis and the solid state structures of $[HIr_5(CO)_{12}]^{2-}$ and $[HIr_4(CO)_{10}(PPh_3)]^-$. *J. Cluster Sci.* **2001**, *12*, 23.

(33) (a) Cifeuntes, M. P.; Humphrey, M. G.; Willis, A. C. High nuclearity ruthenium carbonyl cluster chemistry. 4. Reactivity of $[Ru_{10}(\mu\text{-}H)(\mu_6\text{-}C)\ (CO)_{24}]^-$ towards trimethylphosphite or bis-(diphenilphoshino)acetylene; X-ray crystal structure of $[PPh_4][Ru_{10}(\mu\text{-}H)(\mu_6\text{-}C)\ (CO)_{22}\{P(OMe)_3\}_2]$. *J. Organomet. Chem.* **1996**, *513*, 85. (b) Cifuentes, M. P.; Humphrey, M. G.; Skelton, B. W.; White, A. H. High nuclearity ruthenium carbonyl cluster chemistry. 2. Reaction of $[Ru_2(\mu\text{-}H)(\mu\text{-}NC_5H_4)_2(CO)_4(NC_5H_5)_2][Ru_{10}(\mu\text{-}H)(\mu_6\text{-}C)\ (CO)_{24}]$ with triphenylphosphine. Stepwise apical substitution on a giant tetrahedral cluster. *Organometallics* **1995**, *14*, 1536.

(34) (a) Albano, V. G.; Demartin, F.; Iapalucci, M. C.; Longoni, G.; Sironi, A.; Zanotti, V. Synthesis and X-ray structure of the $[Ni_{13}Sb_2(CO)_{24}]^{n-}$ (n = 2,3,4) cluster anions containing an icosahedral $[Ni_{11}Sb_2(CO)_{18}]^{n-}$ moiety behaving as a distibine ligand and displaying an unexpected electron count. *J. Chem. Soc., Chem. Commun.* **1990**, 547. (b) Albano, V. G.; Demartin, F.; Iapalucci, M. C.; Laschi, F.; Longoni, G.; Sironi, A.; Zanello, P. Icosahedral carbonyl clusters $[Ni_{10}Sb_2(\mu_{12}\text{-}Ni)\ (Ni(CO)_3)_2(CO)_{18}]^{n-}$ (n = 2, 3 or 4). Synthesis, spectroscopic, electrochemical and bonding analysis. Crystal structures of $[Ni_{10}Sb_2(\mu_{12}\text{-}Ni)\ (Ni(CO)_3)_2(CO)_{18}]^{n-}$ (n = 2 or 3). *J. Chem. Soc., Dalton Trans.* **1991**, 739. (c) Albano, V. G.; Demartin, F.; Femoni, C.; Iapalucci, M. C.; Longoni, G.; Monari, M.; Zanello, P. Synthesis and characterization of new paramagnetic nickel carbonyl clusters containing antimony atoms: X-ray structure of $[NEt_3CH_2Ph]_2[Ni_{15}(\mu_{12}\text{-}Sb)\ (CO)_{24}]$ and $[NEt_4]_3[Ni_{10}Sb_2(\mu_{12}\text{-}Ni)(CO)_{18}]$. *J. Organomet. Chem.* **2000**, *593−594*, 325.

(35) Ceriotti, A.; Longoni, G.; Manassero, M.; Masciocchi, N.; Piro, G.; Resconi, L.; Sansoni, M. Synthesis and X-ray structure of $[Ni_{16}(CO)_{23}C_4]^{4-}$. A tetracarbide anionic cluster containing 2-interstitial C_2-fragments. *J. Chem. Soc., Chem. Commun.* **1985**, 1402.

(36) Ciabatti, I.; Femoni, C.; Iapalucci, M. C.; Longoni, G.; Lovato, T.; Zacchini, S. PPh_3-Derivatives of $[Pt_{3n}(CO)_{6n}]^{2-}$ (n = 2−6) Chini's Clusters: Syntheses, Structures, and ^{31}P NMR Studies. *Inorg. Chem.* **2013**, *52*, 4384.

DOI: 10.1021/acs.inorgchem.6b02750
Inorg. Chem. XXXX, XXX, XXX−XXX

(37) Ciabatti, I.; Femoni, C.; Iapalucci, M. C.; Longoni, G.; Zacchini, S. Tetrahedral $[H_nPt_4(CO)_4(P^\wedge P)_2]^{n+}$ (n = 1, 2; P^P = $CH_2{=}C(PPh_2)_2$) Cationic Mono- and Dihydrido Carbonyl Clusters Obtained by Protonation of the Neutral $Pt_4(CO)_4(P^\wedge P)_2$. *Organometallics* **2013**, *32*, 5180.

(38) Heaton, B. T.; Iggo, J. A.; Podkorytov, I. S.; Ponomarenko, V. I.; Selivanov, S. I.; Tunik, S. P. A rare example of a di-cationic hydrido carbonyl tetra-nuclear cluster, $[H_2Rh_2Pt_2(CO)_7(PPh_3)_3]^{2+}$. *Inorg. Chim. Acta* **2010**, *363*, 549.

(39) (a) Ara, I.; Falvello, L. R.; Forniés, J.; Lalinde, E.; Martín, A.; Martínez, F.; Moreno, M. T. Synthesis and structure of new neutral bimetallic platinum hydride complexes. *Organometallics* **1997**, *16*, 5392. (b) Ramachandran, R.; Yang, D.-S.; Payne, N. C.; Puddephatt, R. Phosphine and phosphite complexes of a coordinatively unsaturated triplatinum hydride - Structure of $[Pt_3(m_3\text{-}H)(\mu\text{-}Ph_2PCH_2PPh_2)_3(P(OMe)_3][PF_6]$. *Inorg. Chem.* **1992**, *31*, 4236. (c) Ferguson, G.; Lloyd, B. R.; Puddephatt, R. A platinum cluster complex containing a triply bridging carbonyl. The synthesis and structure of (μ_3-carbonyl)tris[μ-bis(diphenylphosphino)methane]-triangulo-triplatinum(2+) hexafluorophosphate. *Organometallics* **1986**, *5*, 344.

(40) (a) Béni, Z.; Ros, R.; Tassan, A.; Scopelliti, R.; Roulet, R. Synthesis of some pentanuclear platinum clusters $[Pt_5(CO)_6(L)_4]$. The X-ray structure of $[Pt_5(\mu\text{-}CO)_5(CO)\ (PCy_3)_4]$. *Inorg. Chim. Acta* **2005**, *358*, 497. (b) Minghetti, G.; Bandini, A. L.; Banditelli, G.; Bonati, F.; Szostak, R.; Strouse, C. E.; Knobler, C. B.; Kaesz, H. D. Synthesis and Characterization of Cationic Dinuclear Hydridoplatinum Complexes: Crystal and Molecular Structure of $Pt_2(\mu\text{-}H,\mu\text{-}CO)(dpe)_2][BF_4]$ (dpe = 1,2-Bis(diphenylphosphino)ethane. *Inorg. Chem.* **1983**, *22*, 2332. (c) Beringhelli, T.; Ceriotti, A.; D'Alfonso, G.; Della Pergola, R.; Ciani, G.; Moret, M.; Sironi, A. Mixed-Metal Rhenium-Platinum Cluster Compounds. Synthesis and Characterization of Three Isomers of the Triangular Cluster Complex $[Re_2Pt(\mu\text{-}H)_2(CO)_8(PPh_3)_2]$. *Organometallics* **1990**, *9*, 1053.

(41) Pregosin, P. S.; Kunz, R. W. ^{31}P and ^{13}C NMR of Transition Metal Phosphine Complexes. In *NMR Basic Principles and Progress;* Diehl, P., Fluck, E., Kosfeld, R., Eds.; Springer-Veròag: Berlin, Germany, 1979; Vol. *16*.

(42) Budzelaar, P. H. M. *gNMR for Windows,* NMR Simulation Program (5.0.6.0); IvorySoft, Adept Scientific: Letchworth, U.K., 2006.

(43) Hao, L.; Spivak, G. J.; Xiao, J.; Vittal, J. J.; Puddephatt, R. J. First Octahedral Platinum Cluster: Structure as a Function of Electron Count in Pt_6 Clusters. *J. Am. Chem. Soc.* **1995**, *117*, 7011.

(44) (a) Albinati, A. Structural studies of Pt cluster compounds. II. The crystal structure of the trinuclear platinum cluster $Pt_3[P(C_6H_{11})_3(CO)_3$. *Inorg. Chim. Acta* **1977**, *22*, L31. (b) Yoshida, T.; Otsuka, S. Reactions of Two-Coordinate Phosphine Platinum(0) and Palladium(0) Compounds. Ligand Exchange and Reactivities towards Small Molecules. *J. Am. Chem. Soc.* **1977**, *99*, 2134. (c) Burrow, R. A.; Farrar, D. H.; Irwin, J. J. Reactions of the complexes $Pt_3(\mu\text{-}CO)_3L_3$ with SO_2. Crystal structure of $Pt_3(\mu\text{-}CO)_3(P^tBu_2Ph)_3{\cdot}0.25(C_4H_8O)$. *Inorg. Chim. Acta* **1991**, *181*, 65. (d) Ortega-Moreno, L.; Peloso, R.; Maya, C.; Suárez, A.; Carmona, E. Platinum(0) olefin complexes of a bulky terphenylphosphine ligand. Synthetic, structural and reactivity studies. *Chem. Commun.* **2015**, *51*, 17008. (e) Poverenov, E.; Gandelman, M.; Shimon, L. J. W.; Rozenberg, H.; Ben-David, Y.; Milstein, D. Pincer "hemilabile" effect. PCN platinum(II) complexes with different amine "arm length". *Organometallics* **2005**, *24*, 1082.

(45) (a) Cordero, B.; Gómez, V.; Platero-Prats, A. E.; Revés, M.; Echeverría, J.; Cremades, E.; Barragán, F.; Alvarez, S. Covalent radii revisited. *Dalton Trans.* **2008**, 2832. (b) Bondi, A. Van der Waals Volumes and Radii. *J. Phys. Chem.* **1964**, *68*, 441.

(46) (a) Mingos, D. M. P. *Introduction to Cluster Chemistry;* Prentice Hall: Englewood Cliffs, NJ, 1990. (b) Evans, D. G.; Mingos, D. M. P. Polyhedral skeletal electron pair theory: Its extension to non-conical ML_2 fragments. *J. Organomet. Chem.* **1982**, *240*, 321. (c) Evans, D. G. Molecular orbital analysis of the bonding in platinum phosphine hydride clusters. *J. Organomet. Chem.* **1987**, *319*, 265.

(47) (a) Miedaner, A.; Raebiger, J. W.; Curtis, C. J.; Miller, S. M.; DuBois, D. L. Thermodynamic studies of $[HPt(EEtXantphos)_2]^+$ and $[H_2(EtXantphos)_2]^{2+}$. *Organometallics* **2004**, *23*, 2670. (b) Asker, K. A.; Hitchcock, P. B.; Moulding, R. P.; Seddon, K. R. Crystal and molecular structure of bis[1,3-bis(diphenylphosphino)propane] platinum(0). A reevaluation. *Inorg. Chem.* **1990**, *29*, 4146.

(48) (a) Baker, M. J.; Harrison, K. N.; Orpen, A. G.; Pringle, P. G.; Shaw, G. Chelating diphosphite complexes of nickel(0) and platinum(0): their remarkable stability and hydrocyanation activity. *J. Chem. Soc., Chem. Commun.* **1991**, 803. (b) Tominaga, H.; Sakai, K.; Tsubomura, T. Structure and photophysical properties of $[Pt(BINAP)_2]$ [BINAP = 2,2′-bis(diphenylphosphino)-1,1′-bibaphtyl]. *J. Chem. Soc., Chem. Commun.* **1995**, 2273. (c) Berning, D. E.; Noll, B. C.; DuBois, D. L. Relative hydride, proton, and hydrogen atom transfer abilities of $[HM(diphosphine)_2][PF_6]$ complexes (M = Pt, Ni). *J. Am. Chem. Soc.* **1999**, *121*, 11432.

(49) Archirel, P. Redox Properties of the Chini Clusters $[Pt_3(CO)_6]_n^{2-}$ (n = 1−7) in Solution: A Hybrid DFT Study. Application to their Oxidation by O_2. *J. Phys. Chem. C* **2016**, *120*, 8343.

(50) Keller, E. *SCHAKAL99;* University of Freiburg: Germany, 1999.

(51) Sheldrick, G. M. *SADABS,* Program for empirical absorption correction; University of Göttingen: Germany, 1996.

(52) Sheldrick, G. M. *SHELX97,* Program for crystal structure determination; University of Göttingen: Germany, 1997.

DOI: 10.1021/acs.inorgchem.6b02750
Inorg. Chem. XXXX, XXX, XXX−XXX